Zeeman levels of shallow acceptors in cubic semiconductors



1991 J. Phys.: Condens. Matter 3 6789

(http://iopscience.iop.org/0953-8984/3/35/010)

J. Phys.: Condens. Matter 3 (1991) 6789–6815. Printed in the UK

# Zeeman levels of shallow acceptors in cubic semiconductors

W O G Schmitt, E Bangert and G Landwehr

Physikalisches Institut, Universität Würzburg, 8700 Würzburg, Federal Republic of Germany

Received 14 February 1991

**Abstract.** A detailed theory for the Zeeman splitting of shallow acceptors in cubic semiconductors is presented, allowing for cubic contributions from the band structure, magnetic field orientations $\boldsymbol{B} \parallel [001]$, [111], [110] and large magnetic fields $\boldsymbol{B}$. Practically exact solutions are achieved by taking the contributions of higher angular momenta into account. We calculate the Zeeman splitting of the ground state and the first excited odd-parity states. By also determining the probability for transitions between these states we succeed in a reasonable interpretation of the experimental results for Ge and GaAs. We tabulate $g$-values for a wide range of Luttinger parameters. A description of the Zeeman splitting in terms of a linear field dependence only proves to be accurate for limited field strengths.

## 1. Introduction

The electronic states of shallow acceptors in cubic semiconductors have been studied thoroughly in the last two decades both experimentally and theoretically. The pioneering work of Baldereschi and Lipari (1973, 1974), who formulated the acceptor problem in terms of spherical tensor operators, allowed the acceptor states to be calculated with reasonable precision, so that a quantitative interpretation of the experimental results became possible. In the majority of the investigations different acceptor species in germanium and silicon were considered. In these materials various experimental techniques such as infrared absorption (Soepangkat and Fisher 1973, Schubert *et al* 1989, Atzmüller *et al* 1991a,b), photoconductivity (Kirkman *et al* 1978, Broeckx *et al* 1979, Jungwirt and Prettl 1989, Kamiura *et al* 1981), Raman scattering (Said *et al* 1987) and magnetoacoustic attenuation (Tokumoto and Ishiguro 1977) yielded well resolved spectra. All experimental results were interpreted with the help of numerical calculations, which were based on Baldereschi's theory. Excellent agreement was obtained, the central cell corrections of the acceptor ground state were accounted for by using a screened Coulomb potential (Bernholc and Pantelides 1977, Lipari and Baldereschi 1978, Lipari *et al* 1980, Kanehisa and Said 1988).

In more refined investigations the spectral line intensities were successfully analysed by calculating dipole transition matrix elements (Binggeli and Baldereschi 1988, Clauws *et al* 1988). In addition, for uniaxially stressed Ge an accurate theoretical interpretation of far infrared (FIR) data was achieved by introducing the Picus–Bir strain Hamiltonian to the acceptor problem (Broeckx and Vennik 1987, Fisher *et al* 1985, Freeth *et al* 1986). Said *et al* (1986, 1987) applied the acceptor theory to ZnTe

0953-8984/91/356789+27$03.50  

in order to deduce the Luttinger parameters of this material from a comparison of calculated and observed optical acceptor transitions.

The Zeeman splitting of boron and thallium acceptor states in Ge was studied systematically for the first time by Soepangkat and Fisher (1973). In 1979 Broecks *et al* performed quite similar experiments with Al acceptors but achieved a much higher resolution by using photothermal ionization spectroscopy. Jungwirt and Prettl (1989) extended some of these measurements to magnetic fields of about 6 T. For interpreting the data the theory of Bhattacharjee and Rodriguez (1972) was applied. This theory is based on symmetry considerations only, thus relating the Zeeman splitting for different field orientations to one another, but leaving the real $g$-values as adjustable parameters. In addition the theory is restricted to the case of well isolated acceptor levels. This condition is violated, in particular, in Ge for relatively small magnetic fields, where the Zeeman splitting is comparable with the energy separation of neighbouring acceptor levels.

Carbon acceptors in GaAs were investigated by two different groups. In 1978 Kirkman *et al* observed the Zeeman splitting for fields up to 9 T by photoconductivity whereas Schubert *et al* (1989) and Atzmüller *et al* (1991) analysed FIR transmission experiments.

These new and well resolved results have encouraged us to address the old problem of calculating the Zeeman splitting of acceptor states based on the envelope function method. This is a very promising approach, because on the one hand this method gives the correct carbon acceptor states in GaAs with pratically no central cell corrections. On the other hand inserting a magnetic field into the Luttinger matrix is a well established procedure, which has yielded excellent results not only for bulk Landau levels but also in confined two-dimensional hole systems of heterostructures.

The first attempt to calculate $g$-values by Lin-Chung and Wallis (1969) was based on perturbation theory and variational wavefunctions. Lipari and Altarelli (1980) and Broecks and Clauws (1978) introduced a magnetic field in Baldereschi's tensor operators. These were the first proposals for a systematic treatment, however the calculations were rudimentary in nature.

In section 2 of this paper we outline the acceptor model and the mathematical approach for a solution of the problem. First we derive the Zeeman Hamiltonian including terms quadratic in $\boldsymbol{B}$ in a $4 \times 4$ valence band $\boldsymbol{k} \cdot \boldsymbol{p}$ model. Next we show how wavefunctions with the correct symmetry can be constructed for different orientations of the magnetic field $\boldsymbol{B}$ relative to the crystal axes. With these wavefunctions we can construct systems of differential equations acting on the radial parts of the wavefunctions, which determine the energy eigenvalues. After this the numerical procedure for a solution of these systems of equations is presented. The section ends by discussing transition probabilities and selection rules. Consequently, the formalism is applied to the two cubic semiconductors Ge and GaAs in section 3. The substantial experimental data for these materials are analysed in detail in our model calculations. In section 4 we present more general results in form of tables of $g$-values, by which the Zeeman splitting linear in $B$ can be described reasonably well for small fields.

## 2. Acceptor model and mathematical approach

### *2.1. Linear and quadratic Zeeman Hamiltonian*

The key idea for the solution of the shallow acceptor problem is the transformation

of Luttinger's $\boldsymbol{k}\cdot\boldsymbol{p}$ matrix for the kinetic energy of a valence electron into spherical tensor form. This was accomplished first by Baldereschi and Lipari (1973, 1974):

$$H_0 = -k^2 + \mu k^{(2)}\cdot J^{(2)} - \delta \sum_{m=0,\pm 4} a_m (k^{(2)} \times J^{(2)})^{(4)}_m + U(r)$$
$$a_0 = \frac{\sqrt{70}}{5} \qquad a_{\pm 4} = 1 \qquad \mu = \frac{6\gamma_3 + 4\gamma_2}{5\gamma_1} \qquad \delta = \frac{\gamma_3 - \gamma_2}{\gamma_1}. \tag{1}$$

Here we have used the effective Rydberg

$$R_0 = \frac{1}{\varepsilon^2\gamma_1}\frac{e^4 m}{2(4\pi\varepsilon_0)^2\hbar^2}$$

as a unit of energy and the effective Bohr radius $a_0 = \varepsilon\gamma_1 4\pi\varepsilon_0\hbar^2/e^2 m$ as a unit of length. Our definition of spherical tensor operators is somewhat different from that of Baldereschi and Lipari (1973). Given a vector $\boldsymbol{a} = (a_x, a_y, a_z)$, we define our first rank tensor $a^{(1)}$ by

$$a^{(1)}_0 = a_z \qquad a^{(1)}_{\pm 1} = \mp\frac{1}{\sqrt{2}}(a_x \pm \mathrm{i}a_y)$$

(see Edmonds 1960). Higher rank tensors can be successively constructed using Edmond's rule:

$$(A^{(j_1)} \times B^{(j_2)})^{(j_{12})}_{m_{12}} = \sum_{m_1 m_2} \langle j_1 m_1, j_2 m_2 \mid j_{12} m_{12}\rangle A^{(j_1)}_{m_1} B^{(j_2)}_{m_2}.$$

So we get $k^{(2)} := (k^{(1)} \times k^{(1)})^{(2)}$ and $J^{(2)} := (J^{(1)} \times J^{(1)})^{(2)}$. $J$ is the spin-$\frac{3}{2}$ angular momentum operator. The corresponding spinors are the valence band Bloch functions $u^{(J)}_{M_J}$, $M_J = \pm\frac{1}{2}, \pm\frac{3}{2}$ at the $\Gamma$ point of the Brillouin zone.

For the acceptor potential we use the phenomenological approach (Lipari *et al* 1980)

$$U(r) = \frac{2}{r}\left(1 + (\varepsilon - 1)\mathrm{e}^{-\alpha r}\right) \tag{2}$$

where the parameter $\alpha$ can be selected for each impurity so that (1) gives the correct ground state energy. Note that this potential is spherically symmetric, i.e. in ansatz 2 we have not taken into account the fact that the proper symmetry group of the potential of a substitutional impurity is at best $T_d$.

By Hamiltonian (1) we can describe acceptors with ground state energies which are small compared with the energy gap and the spin–orbit splitting. Otherwise more bands have to be taken into account. Therefore, narrow gap semiconductors and Si—for which the spin-orbit splitting is only 44 meV—cannot be treated within this model. In the case of zinc-blende crystals, terms linear in $\boldsymbol{k}$ are possible in $H_0$, but their contribution is negligible (Dresselhaus 1955, Ranvaud *et al* 1979). As a consequence of this and simplifying ansatz (2) the symmetry group of $H_0$ is $O_h$ and not just the subgroup $T_d$.

The effect of an external magnetic field is included by substituting $\boldsymbol{k} \rightarrow \boldsymbol{k} + \boldsymbol{A}$ in Hamiltonian $H_0$ and by adding the standard term $-2(\kappa/\gamma_1)B^{(1)} \cdot J^{(1)}$. We use the gauge

$$\boldsymbol{A} = \frac{1}{2}(\boldsymbol{B} \times \boldsymbol{r}) \hat{=} A^{(1)} = -\frac{\mathrm{i}}{\sqrt{2}}(B^{(1)} \times r^{(1)})^{(1)}.$$

By subsequent application of the angular momentum recoupling scheme (see appendix A) the Hamiltonian can be ordered in terms of different powers of the magnetic field dependence:

$$H = H_0 + H_{\mathrm{lin}} + H_{\mathrm{qua}} \tag{3}$$

$$\begin{aligned} H_{\mathrm{lin}} = B^{(1)} \cdot \Bigg[ & L^{(1)} - \frac{\mu}{2}\sqrt{\frac{5}{3}}(L^{(1)} \times J^{(2)})^{(1)} - \mu\sqrt{\frac{5}{2}}(\mathcal{L}^{(2)} \times J^{(2)})^{(1)} - 2\frac{\kappa}{\gamma_1}J^{(1)} \Bigg] \\ & + \frac{\delta}{2}\sum_{m=0,\pm 4} a_m (B^{(1)} \times [(L^{(1)} \times J^{(2)})^{(3)} - (\mathcal{L}^{(2)} \times J^{(2)})^{(3)} \\ & + \sqrt{5}(\mathcal{L}^{(2)} \times J^{(2)})^{(4)}])^{(4)}_m \end{aligned} \tag{4}$$

$$\begin{aligned} H_{\mathrm{qua}} = & -\frac{1}{2}B^{(0)} \cdot r^{(0)} + \frac{\mu}{4}\sqrt{\frac{5}{3}}B^{(0)} \cdot (r^{(2)} \times J^{(2)})^{(0)} \\ & + \frac{1}{4}B^{(2)} \cdot r^{(2)} + \frac{\mu}{4}\sqrt{\frac{5}{3}}B^{(2)} \cdot [(r^{(0)} \times J^{(2)})^{(2)} - \sqrt{7}(r^{(2)} \times J^{(2)})^{(2)}] \\ & - \frac{\delta}{4\sqrt{3}}\sum_{m=0,\pm 4} a_m (B^{(0)} \times (r^{(2)} \times J^{(2)})^{(4)})^{(4)}_m \\ & - \frac{\delta}{4\sqrt{3}}\sum_{m=0,\pm 4} a_m \Bigg( B^{(2)} \times \Bigg[ (r^{(0)} \times J^{(2)})^{(2)} - \frac{2}{\sqrt{7}}(r^{(2)} \times J^{(2)})^{(2)} \\ & + \sqrt{\frac{5}{2}}(r^{(2)} \times J^{(2)})^{(3)} - \sqrt{\frac{55}{14}}(r^{(2)} \times J^{(2)})^{(4)} \Bigg] \Bigg)^{(4)}_m . \end{aligned} \tag{5}$$

with the abbreviations:

$$L^{(1)} = -\mathrm{i}\sqrt{2}(r^{(1)} \times k^{(1)})^{(1)} \qquad \mathcal{L}^{(2)} = \mathrm{i}(r^{(1)} \times k^{(1)})^{(2)}$$

$$B^{(0)} = (B^{(1)} \times B^{(1)})^{(0)} = -\frac{1}{\sqrt{3}}B^2 \qquad B^{(2)} = (B^{(1)} \times B^{(1)})^{(2)}$$

$$r^{(0)} = (r^{(1)} \times r^{(1)})^{(0)} \qquad r^{(2)} = (r^{(1)} \times r^{(1)})^{(2)}.$$

$L^{(1)}$ is the orbital angular momentum operator. The unit of the magnetic field is $\beta_0 = R_0/\gamma_1\mu_{\mathrm{B}}$.

### *2.2. Wavefunctions of proper symmetry*

The field-independent part $H_0$ contains a dominating spherically symmetric term and a cubic correction proportional to $\delta$ which reduces the symmetry to that of the cubic group $O_h$.

In the case of $\delta = 0$ the angular momentum $L$ of the envelope function and the $J = \frac{3}{2}$ spinors couple to the total angular momentum $\boldsymbol{F} = \boldsymbol{L} + \boldsymbol{J}$ which is a constant of the motion. Parity $\pi$ is also conserved. Therefore an eigenfunction is a linear combination of all the 'spin–orbit parts' $|LJFM_F\rangle$ that are possible for given $F$, $M_F$ and $\pi = (-1)^L$. Using radial functions as expansion coefficients, the wavefunction has the following form:

$$|\Phi_{\pi F M_F}\rangle = \sum_L f_L(r)|LJFM_F\rangle \tag{6}$$

with

$$\langle e_r \mid LJFM_F\rangle = \sum_{M_L M_J} \langle LJFM_F \mid FM_F\rangle Y^L_{M_L} u^{(J)}_{M_J}$$

and $Y^L_{M_L}$ as spherical harmonics.

An example is

$$|\Phi_{\pi \frac{3}{2} M_F}\rangle = f_1(r)|1\tfrac{3}{2}\tfrac{3}{2}M_F\rangle + f_3(r)|3\tfrac{3}{2}\tfrac{3}{2}M_F\rangle.$$

Generally there are two spin–orbit parts for given $F$, $M_F$, $\pi$. For $F = \frac{1}{2}$ there is only one. Consequently we can construct two coupled radial equations ($F \geqslant \frac{3}{2}$) or one radial equation ($F = \frac{1}{2}$). The former are obtained by applying $H_0$ of equation (1) to the ansatz (6) and subsequently multiplying the result from the left by $\langle L'JFM_F|$. Using the Wigner–Eckart theorem and the reduced matrix elements given in appendix B the following differential equations are found:

$$\begin{pmatrix} (1+\alpha_L)\left(\frac{d^2}{dr^2} + \frac{2}{r}\frac{d}{dr} - \frac{L(L+1)}{r^2}\right) + \frac{2}{r} & \beta_L\left(\frac{d^2}{dr^2} + \frac{2L+5}{r}\frac{d}{dr} + \frac{(L+1)(L+3)}{r^2}\right) \\ \beta_L\left(\frac{d^2}{dr^2} - \frac{2L+1}{r}\frac{d}{dr} + \frac{L(L+2)}{r^2}\right) & (1-\alpha_L)\left(\frac{d^2}{dr^2} + \frac{2}{r}\frac{d}{dr} - \frac{(L+2)(L+3)}{r^2}\right) + \frac{2}{r} \end{pmatrix} \times \begin{pmatrix} f_{nL} \\ f_{n,L+2} \end{pmatrix} = E_n \begin{pmatrix} f_{nL}(r) \\ f_{n,L+2}(r) \end{pmatrix} \tag{7}$$

where

$$\alpha_L = -\mu\frac{L+3}{2L+3} \qquad \beta_L = -\mu\frac{\sqrt{3L(L+2)}}{2L+3} \qquad \text{for } F = L + \frac{1}{2}$$

$$\alpha_L = \mu\frac{L}{2L+3} \qquad \beta_L = -\mu\frac{\sqrt{3(L+1)(L+3)}}{2L+3} \qquad \text{for } F = L + \frac{3}{2}$$

$$\alpha_L^2 + \beta_L^2 = \mu^2 \qquad \pi = (-1)^L.$$

For $\delta \neq 0$ $\boldsymbol{F}$ is no longer conserved. Therefore an infinite number of equations of type (7) are coupled by the cubic term of Hamiltonian (1). These large systems can be characterized by the representations $\Gamma^\pi_k$, $\pi = \pm 1$, $k = 6, 7, 8$ of $O_h$, which provide

good quantum numbers. The wavefunctions are linear combinations of all spin–orbit parts $|LJF\Gamma_k m\rangle$, that are possible for given $\Gamma_k^\pi$ and $m$:

$$|\Phi_{\Gamma_k^\pi m}\rangle = \sum_F \sum_L f_{LF}(r)|LJF\Gamma_k m\rangle \tag{8}$$

as for example

$$\begin{aligned}|\Phi_{\Gamma_8^- m}\rangle = {} & f_{1,\frac{1}{2}}(r)|1\tfrac{3}{2}\tfrac{3}{2}\Gamma_8 m\rangle + f_{3,\frac{1}{2}}(r)|3\tfrac{3}{2}\tfrac{3}{2}\Gamma_8 m\rangle \\ & + f_{1,\frac{5}{2}}(r)|1\tfrac{3}{2}\tfrac{5}{2}\Gamma_8 m\rangle + f_{3,\frac{5}{2}}(r)|3\tfrac{3}{2}\tfrac{5}{2}\Gamma_8 m\rangle \\ & + f_{3,\frac{7}{2}}(r)|3\tfrac{3}{2}\tfrac{7}{2}\Gamma_8 m\rangle + f_{5,\frac{7}{2}}(r)|5\tfrac{3}{2}\tfrac{7}{2}\Gamma_8 m\rangle + \cdots .\end{aligned}$$

Herein the cubic spin–orbit parts $|F\Gamma_k m\rangle$ are linear combinations of the $|FM_F\rangle$, that can be found by diagonalizing the matrix

$$C_{M_F' M_F} = \left\langle FM_F' \left| \sum_{m=0,\pm 4} a_m T_m^{(4)} \right| FM_F \right\rangle \Big/ \left\langle F \left\| T^{(4)} \right\| F \right\rangle$$

where $T^{(4)}$ is an arbitrary fourth-rank tensor that operates on the $|FM_F\rangle$. This procedure yields, for example,

$$\begin{aligned}\left|\frac{5}{2},\Gamma_7,\pm\frac{1}{2}\right\rangle &= \frac{1}{\sqrt{6}}\left|\frac{5}{2},\pm\frac{5}{2}\right\rangle - \sqrt{\frac{5}{6}}\left|\frac{5}{2},\mp\frac{3}{2}\right\rangle \\ \left|\frac{5}{2},\Gamma_8,\pm\frac{1}{2}\right\rangle &= \mp\left|\frac{5}{2},\pm\frac{1}{2}\right\rangle \\ \left|\frac{5}{2},\Gamma_8,\pm\frac{3}{2}\right\rangle &= \pm\frac{1}{\sqrt{6}}\left|\frac{5}{2},\pm\frac{3}{2}\right\rangle \pm \sqrt{\frac{5}{6}}\left|\frac{5}{2},\mp\frac{5}{2}\right\rangle .\end{aligned}$$

The phases of the states $|F\Gamma_k m\rangle$ relative to $|F\Gamma_k \tfrac{1}{2}\rangle$ are chosen so that these states transform correctly according to the representations of O, i.e. $\Gamma_8$ states according to $\mathcal{D}^{(3/2)}$, $\Gamma_6$ states according to $\mathcal{D}^{(1/2)}$ and $\Gamma_7$ states according to $\Gamma_2 \cdot \mathcal{D}^{(1/2)}$. The phase of, say, $|F\Gamma_k \tfrac{1}{2}\rangle$ is arbitrary. More generally the spin–orbit part should be labelled $|F\Gamma_k \iota m\rangle$, because for $F \geqslant \frac{9}{2}$ in the decomposition of the full rotation group representation $\mathcal{D}^{(F)}$ the representation $\Gamma_k$ occurs more than once and is therefore numbered by $\iota$.

With ansatz (8) we can again construct the system of coupled radial equations as mentioned earlier, this time by applying $H_0$ including the cubic term and projecting the result on $\langle L'JF'\Gamma_k \iota' m|$. In practice we reduce this system to a finite one by convergence criteria, which are discussed in the next subsection.

When applying an external magnetic field, the symmetry is further reduced. The symmetry group is the common subgroup of $O_h$ and $C_{\infty h}$—the latter is defined by the direction of $\boldsymbol{B}$—i.e. $C_{4h}$ for $\boldsymbol{B} \parallel [001]$, $C_{3i}$ for $\boldsymbol{B} \parallel [111]$ and $C_{2h}$ for $\boldsymbol{B} \parallel [110]$ (see Koster *et al* 1963). The irreducible representations $\Gamma_u^\pi$ of these groups yield good quantum numbers for each orientation of $\boldsymbol{B}$.

We consider first the orientation $\boldsymbol{B} \parallel [001]$. The construction of states which transform according to the irreducible representations $\Gamma_u^\pi$, $u = 5, 6, 7, 8$ of $C_{4h}$ is simple,

because there is a one-to-one correspondence between the components $|LJF\Gamma_k m\rangle$ of the cubic representations and the $\Gamma_u^\pi$ representations (see table 1). Therefore a Zeeman sublevel of symmetry say $\Gamma_5^-$ is a superposition of all possible $\Gamma_6^-$, $m = \frac{1}{2}$ and $\Gamma_8^-$, $m = \frac{1}{2}$ cubic functions:

$$|\Phi_{\Gamma_5^-}\rangle = \sum_L \sum_F \sum_{k=6,8} \sum_\iota f_{LFk\iota}(r)|LJF\Gamma_k^- \iota \tfrac{1}{2}\rangle.$$

Again, for the radial functions $f_{LFk\iota}(r)$ a system of differential equations can be deduced in a similar way as before. It is important to notice that only the individual spin–orbit parts $|LJF\Gamma_k \iota m\rangle$ coincide with the cubic ones—i.e. those of the case $B = 0$—whereas the radial functions depend strongly on the magnetic field strength.

**Table 1.** Relation between the quantum numbers $\Gamma_u$ (representation of a subgroup of O) and the columns of Wigner's $\mathcal{D}$-matrix $\mathcal{D}^{(\alpha)}$ labelled by $m = -\alpha, \ldots, \alpha$, see (9).

| O | $\Gamma_k$ | $\Gamma_6$ | | $\Gamma_7$ | | $\Gamma_8$ | | | |
|---|---|---|---|---|---|---|---|---|---|
| | $m$ | $\frac{1}{2}$ | $-\frac{1}{2}$ | $\frac{1}{2}$ | $-\frac{1}{2}$ | $\frac{3}{2}$ | $\frac{1}{2}$ | $-\frac{1}{2}$ | $-\frac{3}{2}$ |
| $C_4$ | $\Gamma_u$ | $\Gamma_5$ | $\Gamma_6$ | $\Gamma_7$ | $\Gamma_8$ | $\Gamma_8$ | $\Gamma_5$ | $\Gamma_6$ | $\Gamma_7$ |
| $C_3$ | $\Gamma_u$ | $\Gamma_4$ | $\Gamma_5$ | $\Gamma_4$ | $\Gamma_5$ | $\Gamma_6$ | $\Gamma_4$ | $\Gamma_5$ | $\Gamma_6$ |
| $C_2$ | $\Gamma_u$ | $\Gamma_3$ | $\Gamma_4$ | $\Gamma_4$ | $\Gamma_3$ | $\Gamma_4$ | $\Gamma_3$ | $\Gamma_4$ | $\Gamma_3$ |

For the orientations $\boldsymbol{B} \parallel [111]$ and $\boldsymbol{B} \parallel [110]$ the construction of wavefunctions adapted to the symmetry is more complicated, because the field direction is inclined to the [001]-quantization direction of the $|LJF\Gamma_k \iota m\rangle$ spin–orbit parts.

To obtain the correct function for, say, $\boldsymbol{B} \parallel [111]$ one has to transform the $|LJF\Gamma_k \iota m\rangle$ representation into an equivalent representation where the $C_3$-rotation about the [111]-axis is diagonal. This transformation is performed by Wigner's $\mathcal{D}$-matrix $\mathcal{D}^{(\alpha)}(R^{-1})$ as defined by Edmonds (1960), where $R = R(\alpha, \beta, \gamma)$ rotates the [001]-$z$-axis into the [111]-direction ($Re_z = \boldsymbol{B}/B$):

$$|LJF\Gamma_u i\rangle = \sum_{m'=-\alpha}^{\alpha} \mathcal{D}^{(\alpha)}_{m'm}(R^{-1}(\alpha, \beta, \gamma))|LJF\Gamma_k \iota m'\rangle \tag{9}$$

with $(\alpha, k) = (\frac{1}{2}, 6), (\frac{1}{2}, 7), (\frac{3}{2}, 8)$. Generally, in the decomposition of $\mathcal{D}^{(F)}$, $F \geqslant \frac{3}{2}$ a representation $\Gamma_u$, $u = 4, 5, 6$ of $C_{3i}$ occurs more than once. In order to distinguish between them they are numbered by $i = i(k, \iota, m)$. The relationship between the columns $m$ of the matrix $\mathcal{D}^{(\alpha)}$ and the representations $\Gamma_u$ is given in table 1. The Euler angles $\alpha, \beta, \gamma$ are given in table 2. The angle $\gamma$, which influences only the phase of $|LJF\Gamma_u i\rangle$, is chosen in such a way that the matrix elements of all operators contained in the Hamiltonian $H$ are real provided that the components of the cubic spin–orbit parts satisfy the phase relations $\langle F\tfrac{1}{2} \mid F\Gamma_6 \tfrac{1}{2}\rangle$, $\langle F\tfrac{5}{2} \mid F\Gamma_7 \tfrac{1}{2}\rangle$, $\langle F\tfrac{3}{2} \mid F\Gamma_8 \tfrac{3}{2}\rangle > 0$. Again a wavefunction of symmetry $\Gamma_u^\pi$ is a superposition of all possible $|LJF\Gamma_u i\rangle$, $\pi = (-1)^L$ functions built according to (9):

$$|\Phi_{\Gamma_u^\pi}\rangle = \sum_L \sum_F \sum_i f_{LFi}(r)|LJF\Gamma_u i\rangle. \tag{10}$$

**Table 2.** Euler angles for rotations (rotation of the frame of reference, physical system is fixed) that perform the transformation $R(\alpha,\beta,\gamma)e_z = B/B$.

| | $\alpha$ | $\beta$ | $\gamma$ | O-$\Gamma_6,\Gamma_8$ | O-$\Gamma_7$ |
|---|---|---|---|---|---|
| $C_4$ : $R=1$ | 0 | 0 | | 0 | 0 |
| $C_3$ : $R_{111}$ | $\pi/4$ | $\arccos 1/\sqrt{3}$ | | 0 | $\pi$ |
| $C_2$ : $R_{110}$ | $\pi/4$ | $\pi/2$ | | 0 | $\pi$ |

For the orientation $B \parallel [110]$, states which transform according to the representations $\Gamma_3$ and $\Gamma_4$ of the group $C_{2h}$ can be formed by a similar procedure.

The construction of wavefunctions with the correct symmetry for the Zeeman sublevels can be summarized as follows: rotating† the quantization axis of the cubic spin–orbit parts by Wigner's $\mathcal{D}^{(1/2)}$ or $\mathcal{D}^{(3/2)}$ matrices into the direction of the applied magnetic field yields functions of the desired transformation properties. The various radial functions in the ansatz of type (10) are solutions of a complicated and large system of differential equations, which is obtained by applying Hamiltonian $H$ to ansatz (10) and projecting it on $\langle L'JF'\Gamma_u i'|$. This system depends on the magnetic field orientation and the field strength. The coefficients of these differential equations are calculated by a computer program, which, after storing the coefficients, solves the corresponding equations numerically by the method described in the following subsection.

### *2.3. Numerical recipes*

The large systems of coupled differential equations can only be solved numerically. We use neither a variational scheme such as that of Baldereschi and Lipari (1973) nor the finite element method as in Said *et al* (1986) but another technique, the 'matrix method', which has proved to be very efficient for calculating the first few eigenvalues of a large system of differential equations all of which have a similar structure: When combining all $n$ radial functions (e.g. $n = 55$ for $B \parallel [110]$, see later) to a column vector $\psi$, the corresponding $n$ differential equations can be reformulated as $H_R\psi = E\psi$, where $H_R$ is a $n \times n$ matrix operator. Now we expand each radial function into a set of $N$ ($N \approx 20$) basis functions $h_i$. Consequently every matrix element of $H_R$ is expanded into a $N \times N$ matrix. Finally we have to diagonalize the $(nN) \times (nN)$ matrix that corresponds to $H_R$ numerically which can be done by standard procedures (EISPACK).

For our hydrogen-like bound state problem we found the following functions to be most reasonable:

$$h_i^{(\alpha)}(\gamma r) = \gamma^{3/2}\sqrt{\frac{i!}{(\alpha+i)!}}(\gamma r)^{\alpha}\mathrm{e}^{-\gamma r/2}L_i^{(2\alpha+2)}(\gamma r).$$

$L_i^{(\beta)}(x)$ are the generalized Laguerre polynomials. Given the parameters $\alpha, \gamma$, the $h_i$, $i = 0, 1, \ldots$, are complete and orthogonal with respect to the weight function $r^2$. For even-parity states we have to set $\alpha = 0$ whereas for odd-parity states we use $\alpha = 1$, but $\alpha = 0$ will do as well. Using the parameter $\gamma$ we can fit the extension of

† As a rotation of a state $|F\Gamma_k m\rangle$ would cause a rotation of its components by the matrix $\mathcal{D}^{(F)}$, it would be better to use the term 'unitary transformation' instead of 'rotation of the quantization axis' for $F > \frac{3}{2}$.

the functions $h_i^{(\alpha)}(\gamma r)$ to that of the real wavefunctions. $\gamma$ shows a slight dependence on $\mu$ and $\delta$, but neither the eigenvalues nor the eigenfunctions depend on $\gamma$ if it is restricted to a physically relevant interval.

Figure 1 demonstrates that we obtain practically exact eigenvalues from finite instead of infinite matrices. It is shown that by including spin–orbit components with total angular momentum up to $F = \frac{13}{2}$ excellent convergence is achieved for $S_{3/2}$, $P_{3/2}$, $P_{5/2}$ states. This leads to eighteen coupled differential equations for the $\Gamma_8$ states, ten equations for the $\Gamma_7$ states and nine equations for the $\Gamma_6$ states. (Note that the full rotation group representations for $F = \frac{9}{2}$, $F = \frac{11}{2}$, $F = \frac{13}{2}$ decompose into two different $\Gamma_8$ representations each.)

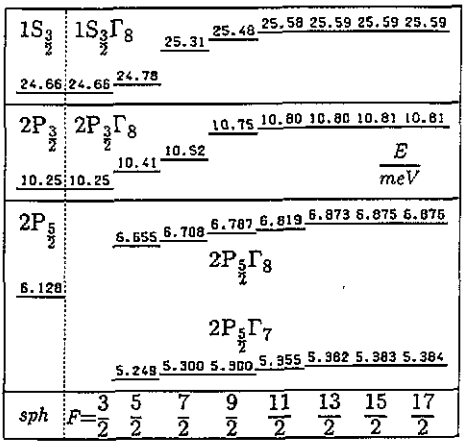


**Figure 1.** Energy levels of the ground state and the first three odd-parity excited states in dependence on the maximal $F$ up to which the sum in equation (8) extends. For comparison the eigenvalues of the states $nL_{\bar{F}}$ in the spherical model are given on the left. Note that 'convergence' is achieved for $F = \bar{F} + 4$. (The Luttinger parameters are those of GaAs.)

For $F \leqslant \frac{13}{2}$ there are all together 110 spin–orbit components for each parity. For $\boldsymbol{B} \parallel [001]$ these functions decompose into 27 functions of symmetry $\Gamma_5$ or $\Gamma_6$, respectively, and 28 of symmetry $\Gamma_7$ or $\Gamma_8$, respectively. As there is no degeneracy for $B \neq 0$, the number of coupled radial equations equals the number of spin–orbit components. So one has to solve systems of 27 or 28 coupled radial equations. For $\boldsymbol{B} \parallel [111]$ the 110 functions decompose into 37 of symmetry $\Gamma_4$ or $\Gamma_5$ and 36 of symmetry $\Gamma_6$, whereas for $\boldsymbol{B} \parallel [110]$ the decomposition is into 55 functions of symmetry $\Gamma_3$ or $\Gamma_4$, respectively.

### *2.4. Transition probabilities and selection rules*

The interaction of a valence band electron with the radiation field is treated as a perturbation. When neglecting second-order terms in the radiation field and using the dipole approximation, we find according to Fermi's Golden Rule the probability for a transition from state $i$ to $f$:

$$w_{if} = \frac{2\pi}{\hbar} e^2 \mathcal{A}^2 \left| \boldsymbol{\varepsilon} \cdot \left\langle f \left| \frac{1}{m_0} \boldsymbol{\pi} \right| i \right\rangle \right|^2 f(E_i) \cdot (1 - f(E_f)) \tag{11}$$

where $\mathcal{A}$ is the modulus of the vector potential $\mathcal{A}$ determined by the radiation field $\boldsymbol{E} = -(\partial/\partial t)\mathcal{A}$, $\boldsymbol{\varepsilon} = \mathcal{A}/\mathcal{A}$ is the polarization vector, $f(E)$ is the Fermi distribution function and $(1/m_0)\pi$ is the velocity operator

$$\frac{1}{m_0}\pi = \frac{1}{m_0}p + \frac{\hbar}{4m_0^2c^2}\sigma \times \nabla V = \frac{\mathrm{i}}{\hbar}[H, r]. \tag{12}$$

In order to evaluate the matrix elements of the velocity operator,which equals $\hbar^{-1}(\partial/\partial k)H^{\mathrm{EMA}}$ in the effective mass approximation (EMA), we make use of the last part of (12):

$$\left\langle f \left| \frac{1}{m_0}\pi \right| i \right\rangle = \frac{\mathrm{i}}{\hbar}(E_f - E_i)\langle f|r|i\rangle$$

where the dipole operator $r$ is simply $r$ times the unit matrix in EMA.

For temperatures $T$ with $kT \ll E_f - E_i$ ($f$ is the ground state; $i$, the odd-parity excited state) the Fermi energy is determined by the equation

$$\sum_{\alpha=1}^{4} f(E_\alpha) = 3$$

with $\alpha$ denoting the four Zeeman sublevels of the $1S_{3/2}\Gamma_8$ ground state. This arises from the fact that three of the four states are occupied by electrons or, to put it in another way, the Fermi level is pinned to the sublevels of $1S_{3/2}\Gamma_8$.

The dipole operator transforms according to the representation $\Gamma_4^-$ of $O_h$ (keep in mind that we use the full cubic group $O_h$ as the symmetry group for $B = 0$). From the matrix elements theorem we find the following selection rules ($B = 0$) for transitions from $\Gamma_k^\pi$ to $\Gamma_{k'}^{\pi'}$, where $\Gamma_k$, $\Gamma_{k'} = \Gamma_6, \Gamma_7, \Gamma_8$ and $\pi, \pi' = \pm 1$:

$$\Gamma_6 \to \Gamma_6 \qquad \Gamma_7 \to \Gamma_7 \qquad \Gamma_8 \to \Gamma_8 \qquad \Gamma_6 \leftrightarrow \Gamma_8 \qquad \Gamma_7 \leftrightarrow \Gamma_8 \qquad \pi\pi' = -1.$$

For $B \neq 0$ we have to distinguish between the different orientations of $\boldsymbol{B}$. Given the representations according to which the three components of $r^{(1)}$ transform (see table 3), we find the selection rules to be as given in table 4. When light propagates in a direction perpendicular to $\boldsymbol{B}$ (Voigt configuration), a transition $\Gamma_i \to \Gamma_f$ is possible for $\boldsymbol{E} \parallel \boldsymbol{B}$ if the matrix element $\langle \Gamma_f | r_0^{(1)} | \Gamma_i \rangle$ does not vanish or for $\boldsymbol{E} \perp \boldsymbol{B}$ if either $\langle \Gamma_f | r_{+1}^{(1)} | \Gamma_i \rangle$ or $\langle \Gamma_f | r_{-1}^{(1)} | \Gamma_i \rangle$ does not vanish. On the other hand, if light propagates in a direction parallel to $\boldsymbol{B}$ (Faraday configuration), a transition $\Gamma_i \to \Gamma_f$ can be observed if either $\langle \Gamma_f | r_{+1}^{(1)} | \Gamma_i \rangle$ (for right-circular polarization) or $\langle \Gamma_f | r_{-1}^{(1)} | \Gamma_i \rangle$ (for left-circular polarization) does not vanish.

**Table 3.** Representations according to which the components of $r^{(1)}$ transform.

| | $r_0$ | $r_+$ | $r_-$ |
|---|---|---|---|
| $C_{4h}$ | $\Gamma_1^-$ | $\Gamma_3^-$ | $\Gamma_4^-$ |
| $C_{3i}$ | $\Gamma_1^-$ | $\Gamma_2^-$ | $\Gamma_3^-$ |
| $C_{2h}$ | $\Gamma_1^-$ | $\Gamma_2^-$ | $\Gamma_2^-$ |

We would like to emphasize that our selection rules are different from those that are obtained when the symmetry group is assumed to be $T_d$ (cf Bhattacharjee and Rodriguez 1972).

## 3. Application to experimentally investigated acceptors

### *3.1. Acceptors in Ge*

Since the Luttinger parameters $\gamma_1$, $\gamma_2$, $\gamma_3$, $\kappa$, of Ge are very well known, it is quite reasonable to test our theory with acceptors in Ge. To obtain the theoretical Zeeman spectrum we use $\gamma_1 = 13.35$, $\gamma_2 = 4.24$, $\gamma_3 = 5.69$, $\kappa = 3.41$, $\varepsilon = 15.36$ as input values and perform numerically all the calculations described earlier. The ground state is computed without the screening term in the potential, i.e. $\alpha = \infty$ in equation (2). As a first result we obtain four $B$-dependent Zeeman levels for the ground state $1S_{3/2}\Gamma_8$ as well as for the excited states $2P_{3/2}\Gamma_8$, $2P_{5/2}\Gamma_8$, $3P_{3/2}\Gamma_8$ and two levels for the excited state $2P_{5/2}\Gamma_7$ (see figure 2). Before discussing the $B$ dependence of these levels in detail, we compare the transition energies between the various Zeeman components according to the selection rules of table 4 with the experimentally observed line positions of FIR spectroscopy. We plotted the results of Soepangkat and Fisher (1973) (lines D and C for polarization $\boldsymbol{E} \parallel \boldsymbol{B}$ and line G) and the better resolved results of Broeckx *et al* (1979) (lines D and C for polarization $\boldsymbol{E} \perp \boldsymbol{B}$). The usual notation for the spectral lines is: G$\hat{=}2P_{3/2}\Gamma_8 \rightarrow 1S_{3/2}\Gamma_8$, D$\hat{=}2P_{5/2}\Gamma_8 \rightarrow 1S_{3/2}\Gamma_8$, C$\hat{=}2P_{5/2}\Gamma_7 \rightarrow 1S_{3/2}\Gamma_8$. Note that for $B > 0$ there may be additional contributions to the split C line from neighbouring Zeeman levels. The experimental values are represented by the broken lines in figure 3. All other lines—full as well as dotted lines—correspond to the calculated energy differences for transitions, which are allowed according to table 4 for the polarizations indicated. The small chemical shift of the Al and B acceptors is suppressed in figure 3, because we found that the Zeeman splitting of the ground state for a finite but large $\alpha$ is about the same as that for $\alpha = \infty$.

Only for the Zeeman multiplet of the D line for the orientation $\boldsymbol{B} \parallel [001]$ and the polarization $\boldsymbol{E} \parallel \boldsymbol{B}$ did the four measured lines correspond to just four allowed transitions. For all other cases there are more allowed than observed transitions. Therefore, a reasonable interpretation of the spectra is possible only if the transition probabilities are calculated additionally and the observed lines are attributed to the strongest transition. The method we used for this calculation is outlined in section 2.4 and the results are indicated in figure 3 as full lines for strong and as dotted lines for weak transitions. Without going into the details the meaning of strong and weak transitions can be explained by two examples. First we consider the G line, $\boldsymbol{B} \parallel [001]$, $\boldsymbol{E} \perp \boldsymbol{B}$ (figure 3($a$), left, bottom). For the eight allowed transitions we found the relative intensities for $B = 2$ T ordered from top to bottom: 49.6, 0.1, 0.0, 29.0, 0.4, 14.6, 6.1 and 0.2%. Noting that the higher of the two observed lines lies just between the strong transitions $7 \rightarrow 6$ (49.6%) and $5 \rightarrow 8$ (29.0%) it was interpreted as the unresolved superposition of these two transitions. Indeed Soepangkat and Fisher (1973) specified an experimental resolution of 0.1 meV, which is as large as the separation of both contributing lines at the highest fields applied. The second observed line is uniquely identified as the $6 \rightarrow 5$ (14.6%) transition, because its energetic position is close to the next strong theoretical line.

This detailed discussion of one of the fourteen spectra of figure 3 shows that a one-to-one interpretation between experimental and theoretical lines is not normally possible, because the finite experimental resolution often merges two or more strong transitions into one line.

As a second example we consider the ten allowed transitions of the D line multiplet with $\boldsymbol{B} \parallel [111]$ and $\boldsymbol{E} \perp \boldsymbol{B}$ for $B = 2$ T (figure 3($b$), left). The relative intensities

**Table 4.** Components of $r^{(1)}$ for which the matrix elements of the form $\langle\Gamma_f|r_m^{(1)}|\Gamma_i\rangle$ can be different from zero for the orientations (*a*) $\boldsymbol{B} \parallel [001]$, (*b*) $\boldsymbol{B} \parallel [111]$ and (*c*) $\boldsymbol{B} \parallel [110]$. $\Gamma_i$ is given in the first row, $\Gamma_f$ is given in the first column.

(*a*)

| $C_4$ | $\Gamma_5$ | $\Gamma_6$ | $\Gamma_7$ | $\Gamma_8$ |
|---|---|---|---|---|
| $\Gamma_5$ | $r_0$ | $r_+$ | 0 | $r_-$ |
| $\Gamma_6$ | $r_-$ | $r_0$ | $r_+$ | 0 |
| $\Gamma_7$ | 0 | $r_-$ | $r_0$ | $r_+$ |
| $\Gamma_8$ | $r_+$ | 0 | $r_-$ | $r_0$ |

(*b*)

| $C_3$ | $\Gamma_4$ | $\Gamma_5$ | $\Gamma_6$ |
|---|---|---|---|
| $\Gamma_4$ | $r_0$ | $r_+$ | $r_-$ |
| $\Gamma_5$ | $r_-$ | $r_0$ | $r_+$ |
| $\Gamma_6$ | $r_+$ | $r_-$ | $r_0$ |

(*c*)

| $C_2$ | $\Gamma_3$ | $\Gamma_4$ |
|---|---|---|
| $\Gamma_3$ | $r_0$ | $r_+, r_-$ |
| $\Gamma_4$ | $r_+, r_-$ | $r_0$ |

of these transitions ordered from top to bottom are: 23.5, 0.1, 9.6, 6.0, 4.5, 0.1, 21.1, 27.1, 0.9 and 7.1%. The highest and the lowest observed transitions can uniquely be assigned to the strong transitions $6_2 \rightarrow 4$ (23.5%) and $4 \rightarrow 6_2$ (7.1%), respectively. The second highest observed line is reasonably interpreted as a superposition of the three transitions: $5 \rightarrow 6_1$ (9.6%), $5 \rightarrow 4$ (6.0%), $5 \rightarrow 6_2$ (4.5%). The remaining third highest observed line is again caused by a superposition of the two transitions $6_1 \rightarrow 5$ (21.1%) and $4 \rightarrow 6_1$ (27.1%). Both individual transitions are very strong, but the experimental resolution of Broeckx *et al* (1979) of 0.06 meV is larger than the separation of these levels.

Both examples show how a careful comparison of theoretical with experimental results can be performed for all the applied magnetic field orientations and polarizations of the light. Since the Luttinger parameters, that are determined from quite different experiments, are the only input values and no fitting parameter is involved, the agreement between experiment and theory can be considered to be excellent.

The most striking results were found for the C line. The Zeeman fans corresponding to the close lying states $2P_{5/2}\Gamma_7$ and $3P_{3/2}\Gamma_8$ merge into one another, so that a large number of allowed transitions appears in a small energy interval. Therefore, it is very satisfactory that the observed lines are only close to the strong transitions. It is clear from our consideration that the Zeeman fan of the C line cannot be attributed only to $2P_{5/2}\Gamma_7$ as stated by Soepangkat and Fisher nor only to $3P_{3/2}\Gamma_8$ as discussed by Broeckx *et al* as it contains both components for finite magnetic fields. Indeed, on analysing the character of the wavefunctions, a strong mixture of the $\Gamma_8$ and $\Gamma_7$ *contributions was found.*

From these results it is evident that the magnetic-field-dependent effective mass description of the acceptor works very well.

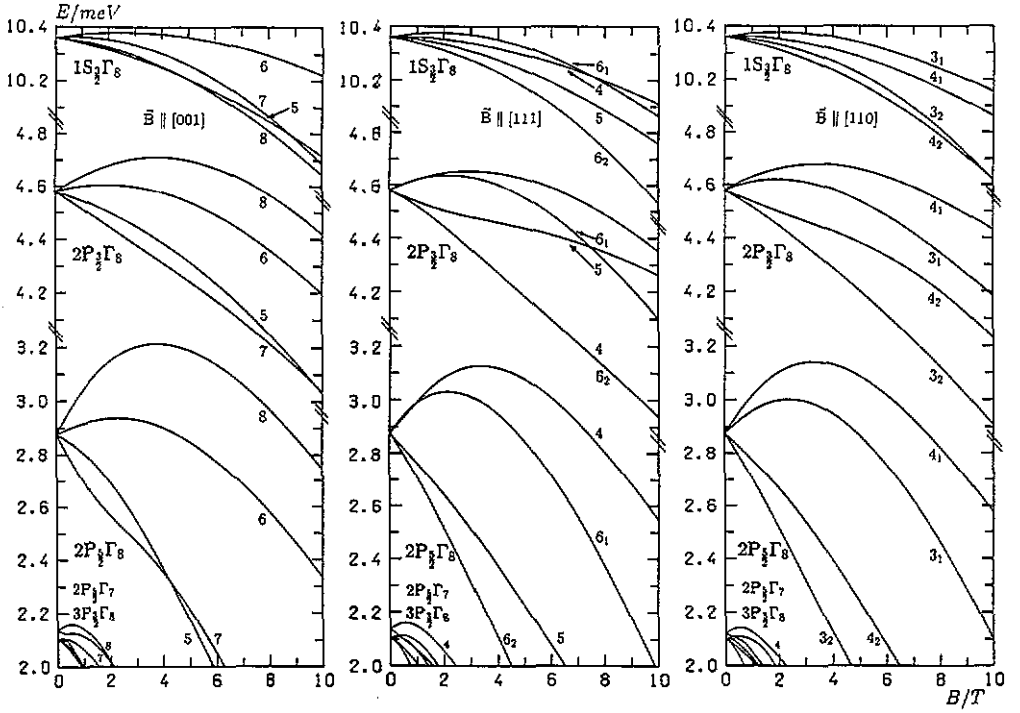


**Figure 2.** Zeeman levels of the ground state and the first few excited states of odd-parity against magnetic field for the three main symmetry orientations. For $B = 0$ Baldereschi's notation is used. For $B > 0$ the Zeeman levels are denoted according to the irreducible representations: $\Gamma_5^\pi$, $\Gamma_6^\pi$, $\Gamma_7^\pi$, $\Gamma_8^\pi$, of $C_{4h}$ for $\boldsymbol{B} \parallel [001]$; $\Gamma_4^\pi$, $\Gamma_5^\pi$, $\Gamma_6^\pi$, of $C_{3i}$ for $\boldsymbol{B} \parallel [111]$; and $\Gamma_3^\pi$, $\Gamma_4^\pi$, of $C_{2h}$ for $\boldsymbol{B} \parallel [110]$. For convenience $\Gamma_u^\pi$ is abbreviated by $u$.

In figure 2 we present the Zeeman levels for the three orientations $\boldsymbol{B} \parallel [001]$, $\boldsymbol{B} \parallel [111]$, $\boldsymbol{B} \parallel [110]$ of the ground state and the first few excited states for field strengths up to 10 T as the main result of our calculation. The anisotropy of the valence band is clearly visible in the acceptor spectrum when the different field orientations are compared. The Zeeman splitting of the ground state for $B = 3$ T is only about one-third of that of the first and one-sixth of that of the second excited state, but it is comparable with the separation of neighbouring levels of the excited states. Therefore, an interpretation of the infrared spectra based on the assumption of negligible ground state splitting, which was proposed by several authors, is not tenable and will not result in a unique assignment of the observed lines to the theoretically predicted transitions.

An exception from this general rule is the Zeeman fan of the D line. A glance at figure 3 shows that the unresolved transitions might be attributed to an unsplit ground state. Therefore, from their careful analysis of the D line, Broeckx *et al* found the correct line assignments and deduced $g$-values for the $2P_{5/2}\Gamma_8$ level, which differ only about 20% from our calculated results:

$$\text{Experimentally deduced values} \left\{ \begin{matrix} g_1' = 8.2 \\ g_2' = 4rg_1' = -3.97 \end{matrix} \right\} \xrightarrow{\text{BT}} \left\{ \begin{matrix} g_1' = 2.76 \\ g_2' = -2.29 \end{matrix} \right\}$$

Calculated values (our theory) $\left\{ \begin{array}{l} g_1' = 2.14 \\ g_2' = -1.86 \end{array} \right\}$

where BT means Bleaney's transformation (Bleaney 1959), which is necessary because Broeckx *et al* (1979) used the $T_d$ notation, whereas for our theory we applied the $O_h$ notation. For the calculation of $g$-values see section 4.

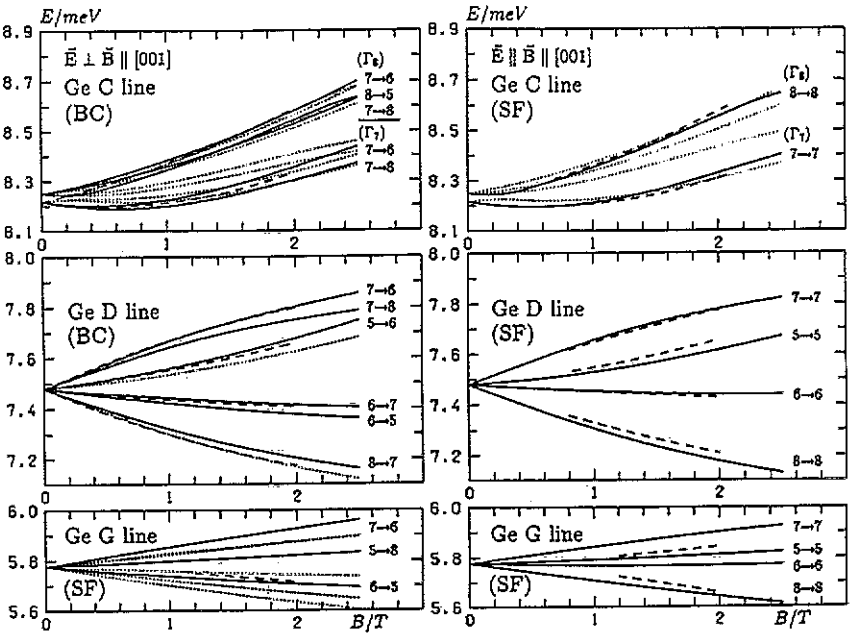


**Figure 3.** Calculated line spectrum (full and dotted lines) against magnetic field for the Ge G, D and C lines. Broken lines refer to the experimental data of Soepangkat and Fisher 1973 (SF) or Broeckx *et al* 1979 (BC). (*a*) $\boldsymbol{B} \parallel [001]$.

Finally we would like to point out the very remarkable fact that the linear dependence of the Zeeman levels on the magnetic field is restricted to very small magnetic fields. Excluding the highest indicated states $2P_{5/2}\Gamma_7$ and $3P_{3/2}\Gamma_8$ a linear dependence yields a quantitative description only up to about 1 T. For the orientation $\boldsymbol{B} \parallel [111]$ this range is even much smaller as can be hypothesized from the fact that the linear Zeeman splitting is symmetric with respect to the $B = 0$ level and this symmetry has already disappeared close to $B = 0$. Thus, we conclude that a description of the Zeeman effect in terms of $g$-values has limited significance. Furthermore, we tried to describe the Zeeman levels in terms of linear and quadratic $B$ dependences according to the formulae of Bhattacharjee and Rodriguez (1972) for the different field orientations. It was found that for all states—including the ground state—and fields of about 10 T the calculated Zeeman spectrum is a long way outside the range of validity of this theory.

### *3.2. Acceptors in GaAs*

For acceptors in GaAs, the literature offers experimental Zeeman spectra obtained by two groups. Kirkman *et al* (1978) published photoconductivity data for the D and C

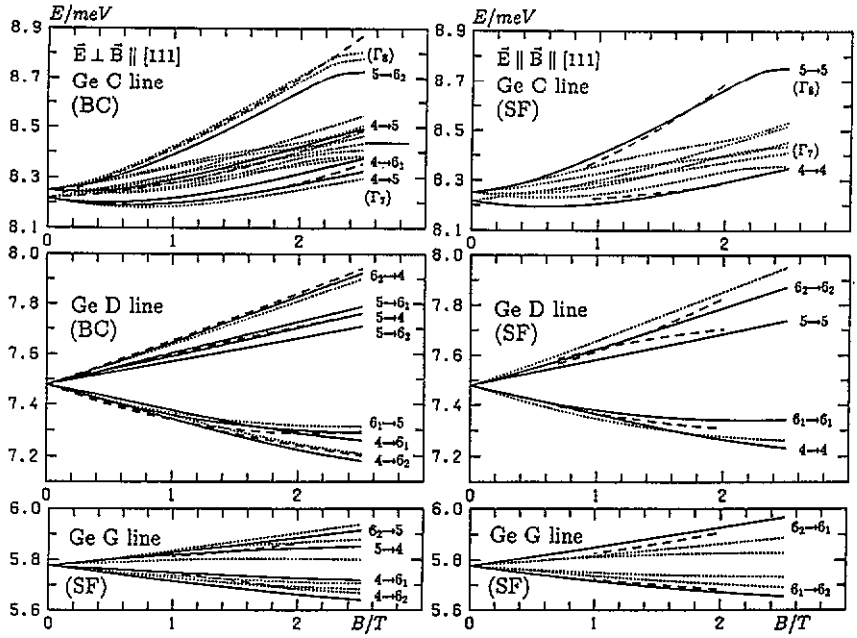


**Figure 3.** (*b*) $\boldsymbol{B} \parallel [111]$.

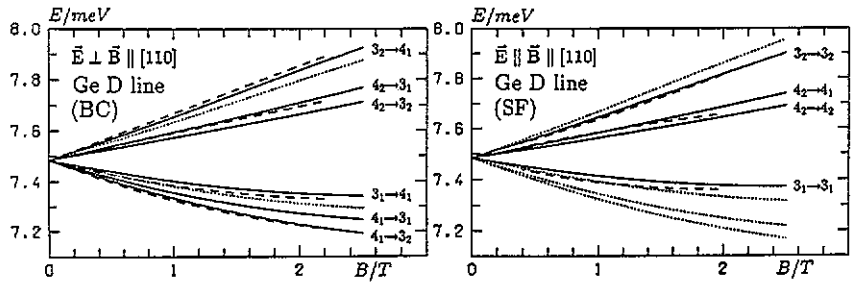


**Figure 3.** (*c*) $\boldsymbol{B} \parallel [110]$.

line for magnetic fields of orientation [001] and strengths up to 9 T. The Würzburg group (Schubert *et al* 1989, Atzmüller *et al* 1991a,b) presented a more complete set of data from transmission experiments for the three orientations $\boldsymbol{B} \parallel [001]$, $\boldsymbol{B} \parallel [111]$ and $\boldsymbol{B} \parallel [110]$ and fields up to 7 T. In particular the Zeeman splitting of the GaAs G line is resolved for the first time by this group. Both groups studied the carbon acceptor, which is suitable for comparisons with theoretical results because of its negligible central cell correction so that the bare Coulomb potential can be used for the potential energy in equation (2).

These acceptors in GaAs have a binding energy which is larger by a factor of about 2.5 than that in Ge. Therefore, the wavefunctions are less extended and lead to smaller Zeeman splittings. This disadvantage is compensated for by the higher magnetic fields which were applied experimentally, so that, because of almost equal resolutions, the experimental information on both systems is equivalent. From the theoretical point of view there is an essential difference between both systems because

the Luttinger parameters $\gamma_1$, $\gamma_2$, $\gamma_3$, $\kappa$, of GaAs are not known as precisely as those of Ge. This is very important because the Zeeman splitting depends in a sensitive manner on these parameters. Utilizing this dependence we proceed as follows: first we select a few lines of the Zeeman spectrum, which are clearly resolved experimentally and can be attributed uniquely to transitions between definite sublevels. Then we fit the calculated line positions of these transitions to the measured ones by optimizing the Luttinger parameters. Finally we compare all the other absorption lines with our calculations based on the deduced parameters.

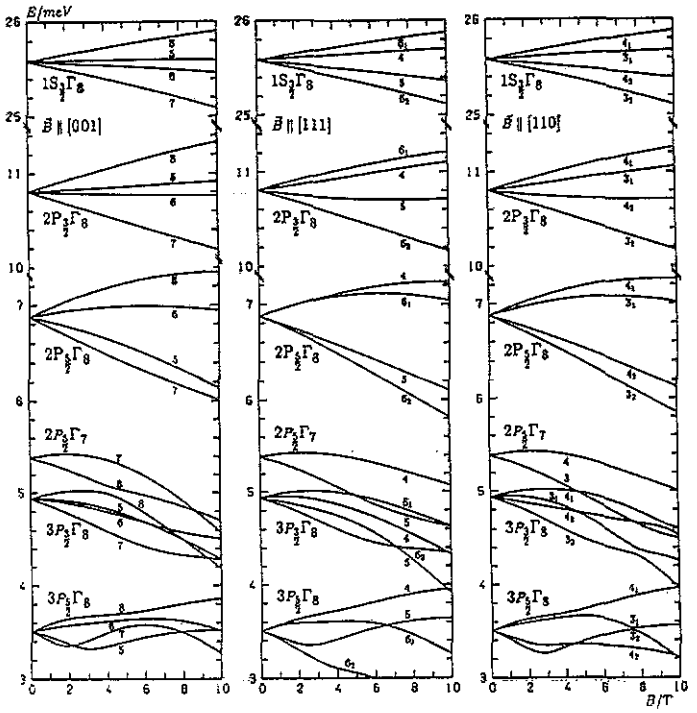


**Figure 4.** Zeeman levels of the ground state and the first few excited states of odd-parity against magnetic field for the three main symmetry orientations.

By presenting some examples we will demonstrate how suitable transitions can be selected. Figure 5 presents the Zeeman components of the G line ($2P_{3/2}\Gamma_8 \rightarrow 1S_{3/2}\Gamma_8$) for orientation $\boldsymbol{B} \parallel [110]$ and polarization $\boldsymbol{E} \perp \boldsymbol{B}$. The corresponding transition probabilities which were calculated according to equation (11), are shown in figure 6. The curves contain the magnetic field dependence of both the dipole matrix elements as well as the level occupation. The transition $3_1 \rightarrow 4_1$ is the strongest one and therefore it is associated with the observed component B in the spectrum for 7 T shown in the insert of figure 6. The level $4_1$ (symmetry $\Gamma_4$) can be identified from figure 4 as the ground state of the acceptor. This fact is responsible for the strong increase in the transition probability with increasing magnetic field. The second intense transition $4_2 \rightarrow 3_1$ is attributed to the observed component C. More information about the line intensities for different magnetic fields is shown in Schubert *et al* (1989). As one further line, which enters our fitting procedure, we consider the transition $3_2 \rightarrow 4_1$ of the split D line ($2P_{5/2}\Gamma_8 \rightarrow 1S_{3/2}\Gamma_8$) described in figures 7 and 8. This is by far

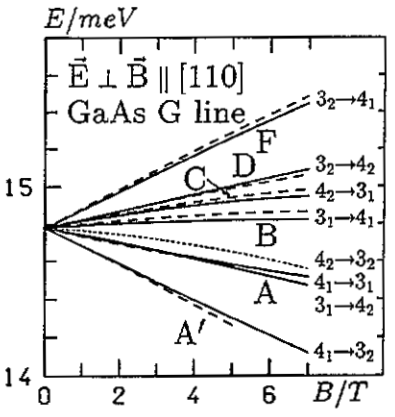


**Figure 5.** Calculated line spectrum (full and dotted lines) against magnetic field for the GaAs G line, $\boldsymbol{E} \perp \boldsymbol{B} \parallel [110]$. Broken lines and capital letters refer to the experimental data of Schubert *et al.*

the strongest transition and therefore associated with the observed component e. In addition this line has the largest transition energy of the D line fan, thus supporting our interpretation of it as a transition between both extreme Zeeman levels of the $1S_{3/2}\Gamma_8$ and $2P_{3/2}\Gamma_8$ states as can be seen from figure 4.

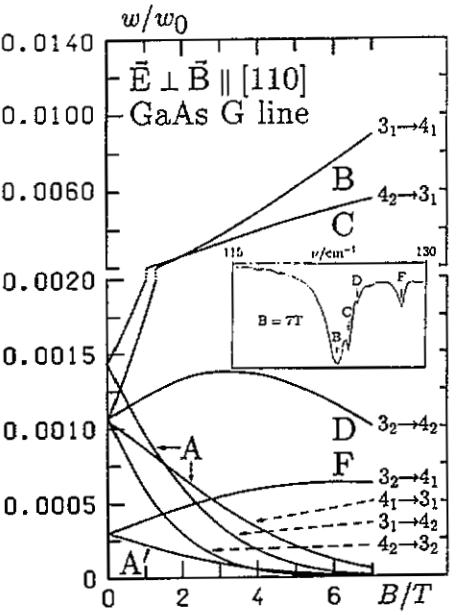


**Figure 6.** Transition probability $w_{if}/w_0 = (E_f - E_i)x_{if}f(E_i)(1 - f(E_f))$ (in au) against magnetic flux density for the GaAs G line, $\boldsymbol{E} \perp \boldsymbol{B} \parallel [110]$. The insert shows an experimental spectrum of Schubert *et al.*

After selecting eight further line components for the other orientations by similar considerations, we performed the parameter determination by an extensive numerical calculation and obtained the values given in table 5. The difference $\gamma_3 - \gamma_2 = 0.68$,

which defines the magnitude of the anisotropy of the valence band, is in good agreement with the results of other experiments. The value $\gamma_1 = 6.65$ is smaller than all the others, but close to the latest ones. The value $\kappa$ was not varied in our fitting procedure, but nevertheless it closely obeys the relation $\gamma_1 - 2\gamma_2 - 3\gamma_3 + 3\kappa + 2 = 0$ (Trebin *et al* 1979), which proves that our parameters are reliable. Recently Said and Kanehisa (1990) published Luttinger parameters (see table 5) extracted from exciton energies that are quite different from our results. As the excitonic spectrum is dominated by the small effective electron mass, their determination is indirect. Indeed their reproduction of the acceptor spectrum directly measured by infrared spectroscopy is less accurate using their parameters than ours.

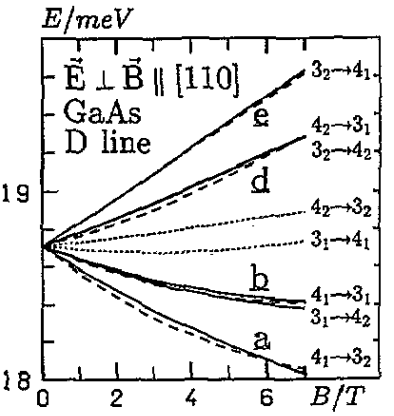


**Figure 7.** Calculated line spectrum (full and dotted lines) against magnetic field for the GaAs D line, $E \perp B \parallel [110]$. Broken lines and underlined letters refer to the experimental data of Atzmüller *et al* 1991a.

**Table 5.** Sets of Luttinger parameters from some other authors in comparison with our values for GaAs. Furthermore, we use $\varepsilon = 12.56$.

| Authors | $\gamma_1$ | $\gamma_2$ | $\gamma_3$ | $\kappa$ |
|---|---|---|---|---|
| Vrehen 1968 | 7.2 | 2.5 | 2.5 | 1.1 |
| Seisyan *et al* 1973 | 7.1 | 2.32 | 2.54 | — |
| Hess *et al* 1976 | 6.85 | 2.1 | 2.9 | 1.2 |
| Skolnick *et al* 1976 | 6.98 | 2.2 | 2.88 | 1.2 |
| Neumann *et al* 1988 | 7.17 | 2.88 | 2.91 | 1.81 |
| Molenkamp *et al* 1988 | 6.79 | 1.924 | 2.681 | — |
| Jäkel 1989 | 6.98 | 2.06 | 2.9 | 1.1 |
| Heuring 1990 | 6.79 | 1.92 | 2.64 | 1.2 |
| Present work | 6.65 | 1.95 | 2.63 | 1.1 |
| Said and Kanehisa 1990 | 7.20 | 2.15 | 3.05 | — |

Now, let us describe the results based on our Luttinger parameters. The overall energy spectrum of a Coulomb-like acceptor in GaAs is shown quantitatively in figure 9. The first twenty energy levels are drawn for each representation and some are labelled according to the notation introduced by Baldereschi and Lipari (1974). Testing the sequence of the levels over the physically relevant Luttinger parameter

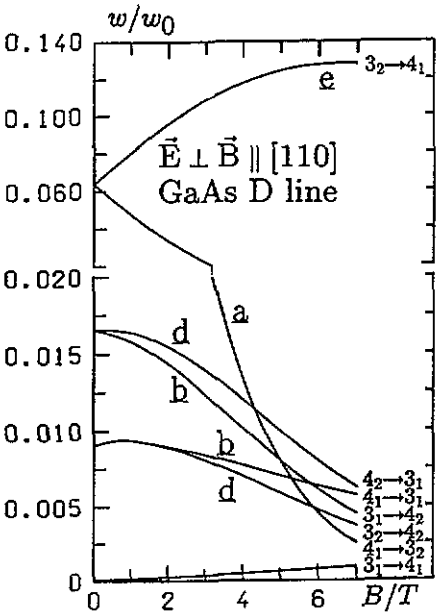


**Figure 8.** Transition probability $w_{if}/w_0 = (E_f - E_i)x_{if}f(E_i)(1 - f(E_f))$ (in au) against magnetic flux density for the GaAs D line, $\boldsymbol{E} \perp \boldsymbol{B} \parallel [110]$. The underlined letters refer to the experimental data of Atzmüller *et al* 1991a.

intervals, we found that only from $1S_{3/2}\Gamma_8$ down to $2P_{5/2}\Gamma_8$ was the ordering of the levels the same for all semiconductors.

Next we consider the plots of the energy spectra against magnetic fields of up to 10 T for the three main orientations which are shown in figure 4. Again the anisotropy of the system is clear. For the ground state and the first two excited states the Zeeman sublevels are nearly linear or only slightly curved. This is different from the Ge case and is caused by the smaller values of $\varepsilon_0$ and $\gamma_1$, which enter the theory in the form of the scaling parameters in $R_0$ and $\beta_0$ defined in section 2.1. Another difference from Ge is that the sequence of the levels is sometimes changed. For instance the ordering of the sublevels of the Ge ground state is $\Gamma_6$, $\Gamma_7$, $\Gamma_8$, $\Gamma_5$ for 1 T in contrast to GaAs, where the sequence is $\Gamma_8$, $\Gamma_5$, $\Gamma_6$, $\Gamma_7$. This clearly demonstrates that the Zeeman splitting is sensitive to small variations in the Luttinger parameters ($(\mu_{Ge} - \mu_{GaAs})/\mu = 7\%$, $\Delta\delta/\delta = 6\%$). Whereas the Zeeman splitting of the first three levels is compatible with experimental results (see later), the residual levels are theoretical predictions.

Finally we compare the theoretically calculated and measured Zeeman spectra. A restriction to the polarization $\boldsymbol{E} \perp \boldsymbol{B}$ is reasonable because in this case more and better resolved lines are observed than for $\boldsymbol{E} \parallel \boldsymbol{B}$. In figures 5, 7 and 10 full curves correspond to calculated strong transitions and dotted lines to calculated weak transitions, whereas the broken lines indicate experimentally determined Zeeman fans.

To begin with, we consider the G line for $\boldsymbol{B} \parallel [110]$ (figure 5). The strongest lines B, C (see figure 6) have already been used for our parameter determination. Transitions D and F are nearly independent of the magnetic field strength. This fact is reasonably well confirmed by experiment (Schubert *et al* 1989). Line A consists of two unresolved transitions. As is shown in figure 6, their intensities as well as that of line $A'$ decrease strongly with increasing magnetic fields. This behaviour is roughly

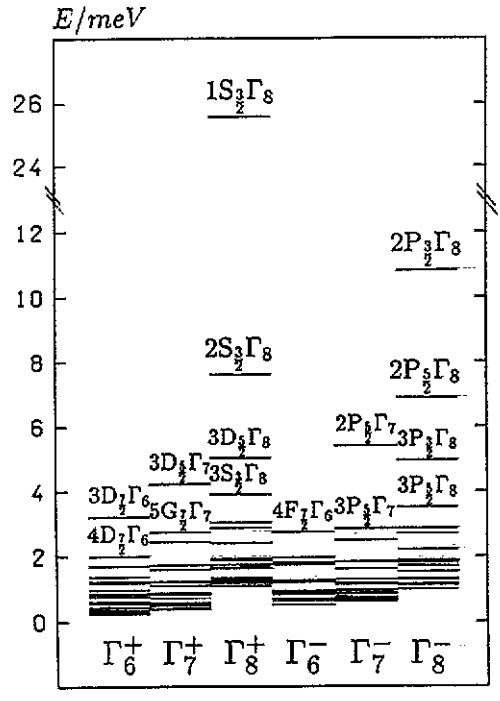


**Figure 9.** Overall energy spectrum of GaAs ($B = 0$) for a Coulomb-like acceptor. For each representation $\Gamma_k^\pi$ of $O_h$ the first twenty levels are drawn. Some of them are denoted according to Baldereschi and Lipari.

the same as that recorded in the experiments.

Without going into the details, we would like to point out that in all other cases the agreement between theoretical and experimental line intensities is similar to the example just discussed explicitly.

In figures 7 and 10 we present a comparison between the calculated and measured Zeeman fans. It is remarkable that for each calculated transition with a large transition probability there is just one experimental line. In the D line fans two close-lying transitions merge into one another and contribute to a single line three times. The experimental D line spectra coincide satisfactorily with our calculated line positions. Concerning the G line we find a similar coincidence except for the components Y ($\boldsymbol{B} \parallel [001]$) and T ($\boldsymbol{B} \parallel [111]$). Both lines cannot be attributed to a *strong* transition. Component Y lies close to the weak transition $7 \rightarrow 8$. In fact, the reason for the appearance of these extra lines is not clear. From the theoretical point of view this can neither be explained by a more accurate determination of the Luttinger parameters nor by screening the Coulomb potential, because the line intensities do not depend strongly on the Luttinger parameters or the screening length.

## 4. $g$-values of acceptor states

Up to now we have applied our theory to two materials by using two special sets of parameters. The accurate description of the extensive experimental results encourages us to present a more general application of our model calculations. For the physically relevant parameter interval we compute the simplest quantities which allow the

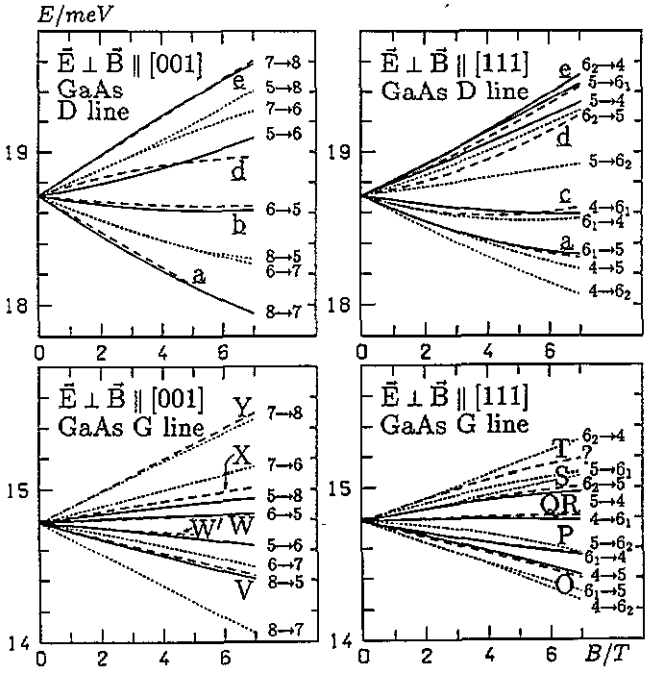


**Figure 10.** Calculated line spectrum against magnetic field for the GaAs G (Schubert *et al*) and D line (Atzmüller *et al* 1991a). Broken lines refer to experimental data.

Zeeman splitting of the fourfold degenerate states $1S_{3/2}\Gamma_8$, $2P_{3/2}\Gamma_8$, $2P_{5/2}\Gamma_8$—the $g$-values—to be described.

By these values one can obtain a survey of the splitting pattern. A more accurate description is possible only by listing higher order coefficients for each parameter set, each Zeeman sublevel and each orientation (see section 3.1, last paragraph).

The $g$-values, $g_m$, $m = \frac{1}{2}, \frac{3}{2}$ are defined and calculated by

$$\langle \Phi_{\Gamma_8^\tau m} | H_{\text{lin}}(\boldsymbol{B} \parallel [001]) | \Phi_{\Gamma_8^\tau m} \rangle = m g_m \mu_B B \tag{13}$$

where $\Phi_{\Gamma_8^\tau m}$ is given by equation (8) and the (reduced) Hamiltonian $H_{\text{lin}}$ by equation (4). The $g_m$ can be obtained as

$$g_m = \gamma_1 \, g_{m,1} + \kappa g_{m,2} \qquad m = \tfrac{1}{2}, \tfrac{3}{2}$$

from the tables 6, 7 and 8, where $g_{m,1}$ and $g_{m,2}$ are listed independently of $\mu$ and $\delta$.

The right-hand side of equation (13) directly gives the linear Zeeman effect for the orientation $\boldsymbol{B} \parallel [001]$. For $\boldsymbol{B} \parallel [111]$, $\boldsymbol{B} \parallel [110]$ one has to calculate the Rodriguez quantities $g_1'$, $g_2'$ (Bhattacharjee and Rodriguez 1972) by the following relations:

$$g_1' = \tfrac{9}{8} g_{1/2} - \tfrac{1}{8} g_{3/2}$$
$$g_2' = -\tfrac{1}{2} g_{1/2} + \tfrac{1}{2} g_{3/2}.$$

These quantities allow us to evaluate the splitting by the more complicated formulae

Table 6. Energy (in au) and $g$-values $g_{m,1}$ and $g_{m,2}$ (for a description see text) for the ground state $1S_{3/2}\Gamma_8$.

| $\mu$ | $\delta$ | $E$ | $g_{\frac{1}{2},1}$ | $g_{\frac{1}{2},2}$ | $g_{\frac{3}{2},1}$ | $g_{\frac{3}{2},2}$ |
|---|---|---|---|---|---|---|
| 0.65 | 0.00 | 1.6534 | 0.2909 | −1.6953 | 0.2909 | −1.6953 |
| 0.65 | 0.05 | 1.6642 | 0.2796 | −1.7623 | 0.2895 | −1.6837 |
| 0.65 | 0.10 | 1.6965 | 0.2611 | −1.8185 | 0.2837 | −1.6654 |
| 0.65 | 0.15 | 1.7522 | 0.2363 | −1.8657 | 0.2734 | −1.6407 |
| 0.65 | 0.20 | 1.8357 | 0.2065 | −1.9053 | 0.2583 | −1.6096 |
| 0.65 | 0.25 | 1.9549 | 0.1736 | −1.9390 | 0.2382 | −1.5717 |
| 0.70 | 0.00 | 1.8570 | 0.3372 | −1.6430 | 0.3372 | −1.6430 |
| 0.70 | 0.05 | 1.8725 | 0.3321 | −1.7210 | 0.3347 | −1.6294 |
| 0.70 | 0.10 | 1.9192 | 0.3201 | −1.7862 | 0.3269 | −1.6081 |
| 0.70 | 0.15 | 2.0007 | 0.3031 | −1.8411 | 0.3136 | −1.5793 |
| 0.70 | 0.20 | 2.1256 | 0.2831 | −1.8882 | 0.2944 | −1.5428 |
| 0.70 | 0.25 | 2.3110 | 0.2631 | −1.9308 | 0.2688 | −1.4982 |
| 0.75 | 0.00 | 2.1450 | 0.3856 | −1.5856 | 0.3856 | −1.5856 |
| 0.75 | 0.05 | 2.1694 | 0.3892 | −1.6778 | 0.3814 | −1.5694 |
| 0.75 | 0.10 | 2.2432 | 0.3867 | −1.7544 | 0.3706 | −1.5439 |
| 0.75 | 0.15 | 2.3748 | 0.3809 | −1.8196 | 0.3529 | −1.5094 |
| 0.75 | 0.20 | 2.5852 | 0.3757 | −1.8781 | 0.3275 | −1.4653 |
| 0.75 | 0.25 | 2.9204 | 0.3759 | −1.9382 | 0.2927 | −1.4098 |
| 0.80 | 0.00 | 2.5802 | 0.4351 | −1.5228 | 0.4351 | −1.5228 |
| 0.80 | 0.05 | 2.6236 | 0.4516 | −1.6349 | 0.4284 | −1.5027 |
| 0.80 | 0.10 | 2.7566 | 0.4630 | −1.7272 | 0.4131 | −1.4712 |
| 0.80 | 0.15 | 3.0045 | 0.4748 | −1.8085 | 0.3882 | −1.4279 |
| 0.80 | 0.20 | 3.4375 | 0.4943 | −1.8917 | 0.3515 | −1.3706 |
| 0.80 | 0.25 | 4.2520 | 0.5329 | −2.0123 | 0.2964 | −1.2897 |
| 0.85 | 0.00 | 3.3087 | 0.4845 | −1.4541 | 0.4845 | −1.4541 |
| 0.85 | 0.05 | 3.4024 | 0.5213 | −1.5970 | 0.4737 | −1.4280 |
| 0.85 | 0.10 | 3.7009 | 0.5552 | −1.7154 | 0.4503 | −1.3863 |
| 0.85 | 0.15 | 4.3230 | 0.5998 | −1.8348 | 0.4112 | −1.3259 |
| 0.85 | 0.20 | 5.7288 | 0.6790 | −2.0307 | 0.3427 | −1.2263 |
| 0.90 | 0.00 | 4.7683 | 0.5319 | −1.3789 | 0.5319 | −1.3789 |
| 0.90 | 0.05 | 5.0595 | 0.6056 | −1.5799 | 0.5129 | −1.3410 |
| 0.90 | 0.10 | 6.1227 | 0.6892 | −1.7673 | 0.4706 | −1.2754 |
| 0.90 | 0.15 | 9.7992 | 0.8651 | −2.1876 | 0.3617 | −1.1079 |
| 0.925 | 0.00 | 6.2279 | 0.5538 | −1.3385 | 0.5538 | −1.3385 |
| 0.925 | 0.05 | 6.9030 | 0.6627 | −1.5975 | 0.5266 | −1.2888 |

given in the paper of Bhattacharjee and Rodriguez (1972)†. As a rule of thumb these formulae are useful for magnetic fields up to one-fifth of $\beta_0$.

Because of the importance of Ge and GaAs we give the explicit $g$-values according to equation (14) in table 9.

As the selection rules are different for transitions between states that are characterized by the representations of the group $O_h$ and those characterized by $T_d$, one has to be careful whenever $g$-values determined by authors working with $T_d$ have to be compared with ours (see Atzmüller *et al* 1991a, section 4.2). When taking into account the fact that the Zeeman levels of the ground state $1S_{3/2}\Gamma_8$ are labelled by the same quantum numbers—thus the splitting is described by the same $g$-values—we

† Assuming $O_h$ to be the symmetry group we obtain the same Hamiltonian matrices as Bhattacharjee and Rodriguez did by using $T_d$ as the symmetry group. Therefore, the resulting energy formulae have the same form in both cases.

Table 7. Energy (in au) and $g$-values $g_{m,1}$ and $g_{m,2}$ (for a description see text) for the state $2P_{3/2}\Gamma_8$.

| $\mu$ | $\delta$ | $E$ | $g_{\frac{1}{2},1}$ | $g_{\frac{1}{2},2}$ | $g_{\frac{3}{2},1}$ | $g_{\frac{3}{2},2}$ |
|---|---|---|---|---|---|---|
| 0.65 | 0.00 | 0.6602 | 0.2708 | −1.3236 | 0.2708 | −1.3236 |
| 0.65 | 0.05 | 0.6666 | 0.2899 | −1.6089 | 0.2653 | −1.2843 |
| 0.65 | 0.10 | 0.6858 | 0.2969 | −1.8972 | 0.2549 | −1.2283 |
| 0.65 | 0.15 | 0.7190 | 0.2884 | −2.1762 | 0.2406 | −1.1573 |
| 0.65 | 0.20 | 0.7691 | 0.2627 | −2.4344 | 0.2236 | −1.0744 |
| 0.65 | 0.25 | 0.8417 | 0.2198 | −2.6637 | 0.2050 | −0.9842 |
| 0.70 | 0.00 | 0.7672 | 0.3192 | −1.3079 | 0.3192 | −1.3079 |
| 0.70 | 0.05 | 0.7765 | 0.3421 | −1.6017 | 0.3125 | −1.2676 |
| 0.70 | 0.10 | 0.8045 | 0.3509 | −1.8963 | 0.2998 | −1.2113 |
| 0.70 | 0.15 | 0.8535 | 0.3431 | −2.1810 | 0.2824 | −1.1403 |
| 0.70 | 0.20 | 0.9297 | 0.3178 | −2.4461 | 0.2620 | −1.0574 |
| 0.70 | 0.25 | 1.0460 | 0.2754 | −2.6842 | 0.2397 | −0.9667 |
| 0.75 | 0.00 | 0.9172 | 0.3677 | −1.2917 | 0.3677 | −1.2917 |
| 0.75 | 0.05 | 0.9319 | 0.3991 | −1.6042 | 0.3590 | −1.2490 |
| 0.75 | 0.10 | 0.9764 | 0.4135 | −1.9152 | 0.3428 | −1.1900 |
| 0.75 | 0.15 | 1.0567 | 0.4097 | −2.2163 | 0.3212 | −1.1155 |
| 0.75 | 0.20 | 1.1890 | 0.3876 | −2.4996 | 0.2959 | −1.0276 |
| 0.75 | 0.25 | 1.4124 | 0.3472 | −2.7557 | 0.2689 | −0.9308 |
| 0.80 | 0.00 | 1.1423 | 0.4160 | −1.2751 | 0.4160 | −1.2751 |
| 0.80 | 0.05 | 1.1686 | 0.4633 | −1.6223 | 0.4039 | −1.2276 |
| 0.80 | 0.10 | 1.2498 | 0.4895 | −1.9662 | 0.3825 | −1.1619 |
| 0.80 | 0.15 | 1.4054 | 0.4956 | −2.3030 | 0.3542 | −1.0774 |
| 0.80 | 0.20 | 1.6966 | 0.4814 | −2.6236 | 0.3214 | −0.9757 |
| 0.80 | 0.25 | 2.3373 | 0.4351 | −2.8804 | 0.2884 | −0.8749 |
| 0.85 | 0.00 | 1.5177 | 0.4639 | −1.2578 | 0.4639 | −1.2578 |
| 0.85 | 0.05 | 1.5749 | 0.5409 | −1.6703 | 0.4459 | −1.2009 |
| 0.85 | 0.10 | 1.7609 | 0.5917 | −2.0815 | 0.4152 | −1.1199 |
| 0.85 | 0.15 | 2.1815 | 0.6210 | −2.4961 | 0.3743 | −1.0097 |
| 0.85 | 0.20 | 3.3872 | 0.5957 | −2.8116 | 0.3313 | −0.8990 |
| 0.90 | 0.00 | 2.2685 | 0.5110 | −1.2399 | 0.5110 | −1.2399 |
| 0.90 | 0.05 | 2.4482 | 0.6521 | −1.7930 | 0.4804 | −1.1612 |
| 0.90 | 0.10 | 3.1651 | 0.7667 | −2.3749 | 0.4270 | −1.0343 |
| 0.90 | 0.15 | 7.1278 | 0.7175 | −2.6358 | 0.3738 | −0.9402 |
| 0.92 | 0.00 | 2.8316 | 0.5295 | −1.2324 | 0.5295 | −1.2324 |
| 0.92 | 0.05 | 3.1795 | 0.7214 | −1.8975 | 0.4888 | −1.1352 |
| 0.92 | 0.10 | 5.0477 | 0.8840 | −2.6049 | 0.4147 | −0.9645 |

have to change the labelling for the excited states and thus we must perform Bleaney's transformation (Bleaney 1959) on their $g$-values.

## 5. Summary

A systematic and nearly exact solution of the acceptor problem is achieved by group theoretical considerations and by utilizing the formalism of spherical tensor operators, which allowed the symmetry for the various orientations $\boldsymbol{B}\|[001]$, [111], [110] of the magnetic field to be exploited. The whole treatment works within the representations of the group $O_h$ and its subgroups $C_{4h}$, $C_{3i}$ and $C_{2h}$.

A careful analysis of the convergence including contributions of higher total angular momenta was described. Thus the Hamiltonian could be represented by a finite matrix

Table 8. Energy (in au) and $g$-values $g_{m,1}$ and $g_{m,2}$ (for a description see text) for the state $2P_{5/2}\Gamma_8$.

| $\mu$ | $\delta$ | $E$ | $g_{\frac{1}{2},1}$ | $g_{\frac{1}{2},2}$ | $g_{\frac{3}{2},1}$ | $g_{\frac{3}{2},2}$ |
|---|---|---|---|---|---|---|
| 0.65 | 0.00 | 0.4059 | −0.0731 | −0.8091 | 0.0894 | 0.9889 |
| 0.65 | 0.05 | 0.4231 | −0.1836 | −0.4492 | 0.0899 | 0.9781 |
| 0.65 | 0.10 | 0.4453 | −0.2689 | −0.0847 | 0.0866 | 0.9475 |
| 0.65 | 0.15 | 0.4739 | −0.3252 | 0.2779 | 0.0788 | 0.9005 |
| 0.65 | 0.20 | 0.5112 | −0.3499 | 0.6326 | 0.0656 | 0.8418 |
| 0.65 | 0.25 | 0.5613 | −0.3419 | 0.9782 | 0.0467 | 0.7771 |
| 0.70 | 0.00 | 0.4606 | −0.0217 | −0.7606 | 0.0265 | 0.9296 |
| 0.70 | 0.05 | 0.4827 | −0.1385 | −0.3663 | 0.0273 | 0.9253 |
| 0.70 | 0.10 | 0.5127 | −0.2253 | 0.0292 | 0.0241 | 0.9009 |
| 0.70 | 0.15 | 0.5531 | −0.2806 | 0.4253 | 0.0158 | 0.8605 |
| 0.70 | 0.20 | 0.6089 | −0.3032 | 0.8215 | 0.0013 | 0.8092 |
| 0.70 | 0.25 | 0.6887 | −0.2932 | 1.2217 | −0.0203 | 0.7533 |
| 0.75 | 0.00 | 0.5386 | 0.0296 | −0.7133 | −0.0362 | 0.8718 |
| 0.75 | 0.05 | 0.5690 | −0.1026 | −0.2640 | −0.0360 | 0.8748 |
| 0.75 | 0.10 | 0.6131 | −0.1981 | 0.1823 | −0.0401 | 0.8565 |
| 0.75 | 0.15 | 0.6766 | −0.2589 | 0.6352 | −0.0502 | 0.8223 |
| 0.75 | 0.20 | 0.7713 | −0.2863 | 1.1019 | −0.0683 | 0.7781 |
| 0.75 | 0.25 | 0.9239 | −0.2817 | 1.5907 | −0.0963 | 0.7342 |
| 0.80 | 0.00 | 0.6573 | 0.0798 | −0.6678 | −0.0976 | 0.8163 |
| 0.80 | 0.05 | 0.7037 | −0.0827 | −0.1303 | −0.0997 | 0.8284 |
| 0.80 | 0.10 | 0.7774 | −0.1990 | 0.4003 | −0.1064 | 0.8168 |
| 0.80 | 0.15 | 0.8950 | −0.2782 | 0.9526 | −0.1210 | 0.7889 |
| 0.80 | 0.20 | 1.0989 | −0.3253 | 1.5426 | −0.1476 | 0.7556 |
| 0.80 | 0.25 | 1.5293 | −0.3299 | 2.1374 | −0.1913 | 0.7530 |
| 0.85 | 0.00 | 0.8571 | 0.1284 | −0.6249 | −0.1569 | 0.7637 |
| 0.85 | 0.05 | 0.9406 | −0.0932 | 0.0637 | −0.1641 | 0.7886 |
| 0.85 | 0.10 | 1.0950 | −0.2562 | 0.7482 | −0.1769 | 0.7853 |
| 0.85 | 0.15 | 1.3981 | −0.3852 | 1.4934 | −0.2029 | 0.7680 |
| 0.85 | 0.20 | 2.1960 | −0.4487 | 2.2047 | −0.2567 | 0.8006 |
| 0.90 | 0.00 | 1.2593 | 0.1746 | −0.5848 | −0.2134 | 0.7147 |
| 0.90 | 0.05 | 1.4678 | −0.1761 | 0.4073 | −0.2322 | 0.7616 |
| 0.90 | 0.10 | 2.0064 | −0.4631 | 1.4449 | −0.2613 | 0.7730 |
| 0.90 | 0.15 | 4.4312 | −0.4980 | 2.0384 | −0.3436 | 0.9178 |
| 0.92 | 0.00 | 1.5617 | 0.1925 | −0.5695 | −0.2353 | 0.6961 |
| 0.92 | 0.05 | 1.9235 | −0.2594 | 0.6522 | −0.2630 | 0.7581 |
| 0.92 | 0.10 | 3.2363 | −0.6477 | 1.9544 | −0.3120 | 0.7957 |

Table 9. $g$-values $g_1'$ and $g_2'$ (for a description see text) of the states $1S_{3/2}\Gamma_8$, $2P_{3/2}\Gamma_8$, $2P_{5/2}\Gamma_8$ for Ge and GaAs.

| | Ge | | GaAs | |
|---|---|---|---|---|
| | $g_1'$ | $g_2'$ | $g_1'$ | $g_2'$ |
| $1S_{3/2}\Gamma_8$ | −0.5904 | 0.2257 | 0.2081 | 0.1147 |
| $2P_{3/2}\Gamma_8$ | −1.1339 | 0.8190 | 0.2445 | 0.2093 |
| $2P_{5/2}\Gamma_8$ | −2.1434 | 1.8577 | −1.7068 | 1.2305 |

of differential operators, which was diagonalized numerically by the matrix method. By this procedure we gained energy levels and envelope functions. The latter were used for calculating transition probabilities in the dipole approximation. The selection

rules for transitions between the states of $O_h$, $C_{4h}$, $C_{3i}$ or $C_{2h}$ symmetry were also found by group theoretical means.

By calculating Zeeman sublevels and line intensities for transitions between these levels we were able to present a conclusive interpretation of the experimental data on Ge and GaAs without making use of screening effects for the acceptor potential. For Ge we used Luttinger parameters that are well known from quite different experiments. The agreement between the calculated and experimental results is good for the G and D lines. The splitting of the C line is shown to be very complicated because for finite magnetic fields the initial states are mixtures of the sublevels of $2P_{5/2}\Gamma_7$ and $3P_{3/2}\Gamma_8$. Agreement with experiment is equally good. As the Luttinger parameters for GaAs are not as well known as those for Ge we had to fit the Luttinger parameters to experiment. Our results (see table 5) should be reliable, because (1) the Zeeman splitting depends sensitively on the Luttinger parameters and (2) we could make use of some experimentally determined spectra for different orientations of the magnetic field. Finally the Zeeman splitting of the carbon G and D lines could be explained successfully for GaAs.

We tabulated the $g$-values for a physically relevant interval of Luttinger parameters. From these $g$-values the linear Zeeman splitting of the G and D lines could be approximately calculated at least for magnetic fields up to one-fifth of the corresponding effective unit.

## Appendix

### *A1. Angular momentum recoupling schemes*

When performing the substitution $k^{(1)} \to k^{(1)} - (\mathrm{i}/\sqrt{2})(B^{(1)} \times r^{(1)})^{(1)}$ in Hamiltonian $H_0$ (1) we get an expression with an intricate dependence on the flux density where $B^{(1)}$ is found at the innermost of the multiple brackets. The ordering of these brackets can be altered by applying the angular momentum recoupling formulae that allow us to change between different coupling schemes for three or four angular momenta (e.g. between $|(j_1 j_2) j_{12} j_3, JM\rangle$ and $|j_1 (j_2 j_3) j_{23}, JM\rangle$). For the spherical tensors $A^{(j_1)}$, $B^{(j_2)}$, $C^{(j_3)}$, $D^{(j_4)}$ these formulae read:

$$((A^{(j_1)} \times B^{(j_2)})^{(j_{12})} \times C^{(j_3)})^{(J)} = (-1)^{j_1+j_2+j_3+J} \sum_{j_{23}} \sqrt{(2j_{12}+1)(2j_{23}+1)} \times \begin{Bmatrix} j_1 & j_2 & j_{12} \\ j_3 & J & j_{23} \end{Bmatrix} (A^{(j_1)} \times (B^{(j_2)} \times C^{(j_3)})^{(j_{23})})^{(J)} \tag{A1}$$

$$((A^{(j_1)} \times B^{(j_2)})^{(j_{12})} \times (C^{(j_3)} \times D^{(j_4)})^{(j_{34})})^{(J)} = \sum_{j_{13} j_{24}} \sqrt{(2j_{12}+1)(2j_{34}+1)(2j_{13}+1)(2j_{24}+1)} \begin{Bmatrix} j_1 & j_2 & j_{12} \\ j_3 & j_4 & j_{34} \\ j_{13} & j_{24} & J \end{Bmatrix} \times ((A^{(j_1)} \times C^{(j_3)})^{(j_{13})} \times (B^{(j_2)} \times D^{(j_4)})^{(j_{24})})^{(J)}. \tag{A2}$$

Note that if the components of the operators $B^{(j_2)}$ and $C^{(j_3)}$ do not commute, the operators on the right-hand side of (A2) perform in the original order, i.e. successively $D^{(j_4)}$, $C^{(j_3)}$, $B^{(j_2)}$ and $A^{(j_1)}$.

*A2. Reduced matrix elements*

$$\langle J \| J^{(1)} \| J\rangle = \sqrt{J(J+1)(2J+1)}$$

$$\langle J \| J^{(2)} \| J\rangle = \frac{1}{2\sqrt{6}}\sqrt{(2J-1)2J(2J+1)(2J+2)(2J+3)}$$

$$\langle L' \| r^{(0)} \| L\rangle = -\sqrt{\frac{2L+1}{3}}r^2\delta_{L'L}$$

$$\langle L+1 \| r^{(1)} \| L\rangle = \sqrt{L+1}r$$

$$\langle L-1 \| r^{(1)} \| L\rangle = -\sqrt{L}r$$

$$\langle L+2 \| r^{(2)} \| L\rangle = \sqrt{\frac{(L+1)(L+2)}{2L+3}}r^2$$

$$\langle L \| r^{(2)} \| L\rangle = -\sqrt{\frac{2L(L+1)(2L+1)}{3(2L-1)(2L+3)}}r^2$$

$$\langle L-2 \| r^{(2)} \| L\rangle = \sqrt{\frac{L(L-1)}{2L-1}}r^2$$

$$\langle L' \| k^2 \| L\rangle = -\left[\frac{\mathrm{d}^2}{\mathrm{d}r^2} + \frac{2}{r}\frac{\mathrm{d}}{\mathrm{d}r} - \frac{L(L+1)}{r^2}\right]\delta_{L'L}$$

$$\langle L+2 \| k^{(2)} \| L\rangle = -\sqrt{\frac{(L+1)(L+2)}{2L+3}}\left(\frac{\mathrm{d}^2}{\mathrm{d}r^2} - \frac{2L+1}{r}\frac{\mathrm{d}}{\mathrm{d}r} + \frac{L(L+2)}{r^2}\right)$$

$$\langle L \| k^{(2)} \| L\rangle = \sqrt{\frac{2L(L+1)(2L+1)}{3(2L-1)(2L+3)}}\left(\frac{\mathrm{d}^2}{\mathrm{d}r^2} + \frac{2}{r}\frac{\mathrm{d}}{\mathrm{d}r} - \frac{L(L+1)}{r^2}\right)$$

$$\langle L-2 \| k^{(2)} \| L\rangle = -\sqrt{\frac{L(L-1)}{2L-1}}\left(\frac{\mathrm{d}^2}{\mathrm{d}r^2} + \frac{2L+1}{r}\frac{\mathrm{d}}{\mathrm{d}r} + \frac{(L-1)(L+1)}{r^2}\right)$$

$$\langle L' \| L^{(1)} \| L\rangle = \sqrt{L(L+1)(2L+1)}\delta_{L'L}$$

$$\langle L+2 \| \mathcal{L}^{(2)} \| L\rangle = \sqrt{\frac{(L+1)(L+2)}{2L+3}}\left(r\frac{\mathrm{d}}{\mathrm{d}r} - L\right)$$

$$\langle L \| \mathcal{L}^{(2)} \| L\rangle = -\sqrt{\frac{L(L+1)(2L+1)}{6(2L-1)(2L+3)}}\left(2r\frac{\mathrm{d}}{\mathrm{d}r} + 3\right)$$

$$\langle L-2 \| \mathcal{L}^{(2)} \| L\rangle = \sqrt{\frac{L(L-1)}{2L-1}}\left(r\frac{\mathrm{d}}{\mathrm{d}r} + L + 1\right).$$

## References

Atzmüller R, Dahl M, Kraus J, Schaack G and Schubert J 1991a *J. Phys.: Condens. Matter* **3** 6775

Atzmüller R, Dahl M, Kraus J and Schaack G, Bangert E and Schmitt W O G 1991b Zeeman effect of the carbon acceptor in GaAs II *High Magnetic Fields in Semiconductor Physics III* ed G Landwehr (Berlin: Springer)

Baldereschi A and Lipari N O 1973 *Phys. Rev.* B **8** 2697
—— 1974 *Phys. Rev.* B **9** 1525
Bernholc J and Pantelides S T 1977 *Phys. Rev.* B **15** 4935
Bhattacharjee A K and Rodriguez S 1972 *Phys. Rev.* B **6** 3836
Binggeli N and Baldereschi A 1988 *Solid State Commun.* **66** 323
Bleaney B 1959 *Proc. Phys. Soc.* **73** 939
Broeckx J and Clauws P 1978 *Solid State Commun.* **28** 355
Broeckx J, Clauws P, Van den Steen K and Vennik J 1979 *J. Phys. C: Solid State Phys.* **12** 4061
Broeckx J and Vennik J 1987 *Phys. Rev.* B **35** 6165
Clauws P, Broeckx J, Rotsaert E and Vennik J 1988 *Phys. Rev.* B **38** 12377
Dresselhaus G 1955 *Phys. Rev.* **100** 580
Edmonds A R 1960 *Angular Momentum in Quantum Mechanics* (Princeton: Princeton University Press)
Fisher P, Freeth C A, Martin A D and Simmonds P E 1985 *Solid State Commun.* **53** 1138 (special issue)
Freeth C A, Fisher P and Simmonds P E 1986 *Solid State Commun.* **60** 175
Hess K, Bimberg D, Lipari N, Fishbach J and Altarelli M 1976 *Proc. 13th Int. Conf. on the Physics of Semiconductors (Rome)* ed F G Fumi (Amsterdam: North-Holland) p 142
Heuring W 1990 *Thesis* Universität Würzburg
Jäkel B 1989 *Thesis* Universität Würzburg
Jungwirt G and Prettl W 1989 *Int. J. Infrared and Millimeter Waves* **10** 1033
Kamiura Y, Broeckx J, Clauws P and Vennik J 1981 *Solid State Commun.* **38** 883
Kanehisa M A and Said M 1988 *J. Phys. C: Solid State Phys.* **21** 4637
Kirkman R F, Stradling R A and Lin-Chung P J 1978 *J. Phys. C: Solid State Phys.* **11** 419
Koster G F, Dimmock J O, Wheeler R G and Statz H 1963 *Properties of the Thirty-Two Point Groups* (Cambridge, MA: MIT Press)
Lin-Chung P J and Wallis R F 1969 *J. Phys. Chem. Solids* **30** 1453
Lipari N O and Altarelli M 1980 *Solid State Commun.* **33** 47
Lipari N O and Baldereschi A 1978 *Solid State Commun.* **25** 665
Lipari N O, Baldereschi A and Thewalt M L W 1980 *Solid State Commun.* **33** 277
Molenkamp L, Eppenga R, t'Hooft G, Dawson P, Foxon C and Moore K 1988 *Phys. Rev.* B **38** 4324
Neumann C, Nöthe A and Lipari N O 1988 *Phys. Rev.* B **37** 922
Ranvaud R, Trebin H-R, Rössler U, Pollak F H 1979 *Phys. Rev.* B **20** 701
Said M, Kanehisa M A 1990 *Phys. Status Solidi* b **157** 311
Said M, Kanehisa M A and Balkanski M 1986 *Solid State Commun.* **57** 417
Said M, Kanehisa M A, Jouanne M and Balkanski M 1987 *J. Phys. C: Solid State Phys.* **20** 2917
Schubert J, Dahl M and Bangert E 1989 Zeeman effect of the carbon acceptor in GaAs *High Magnetic Fields in Semiconductor Physics II* ed G Landwehr (Berlin: Springer)
Seisyan R, Abdullaev M and Draznin V 1973 *Sov. Phys. Semicond.* **7** 522
Skolnick M, Jain A, Stradling R, Leotin J, Ousset J and Askenazy S 1976 *J. Phys. C: Solid State Phys.* **9** 2809
Soepangkat H P and Fisher P 1973 *Phys. Rev.* B **8** 870
Tokumoto H and Ishiguro T 1977 *Phys. Rev.* B **15** 2099
Trebin H-R, Rössler U and Ranvaud R 1979 *Phys. Rev.* B **20** 686
Vrehen Q 1968 *J. Phys. Chem. Solids* **29** 129